

Excited Thomas-Efimov levels in ultracold gases

Mark D. Lee

Clarendon Laboratory, Department of Physics, University of Oxford, Parks Road, Oxford, OX1 3PU, UK

Thorsten Köhler

Department of Physics and Astronomy, University College London, Gower Street, London, WC1E 6BT, UK

Paul S. Julienne

*Atomic Physics Division, National Institute of Standards and Technology,
100 Bureau Drive Stop 8423, Gaithersburg, Maryland 20899-8423*

(Dated: June 4, 2018)

Since the early days of quantum physics, the complex behavior of three interacting particles has been the subject of numerous experimental and theoretical studies. In a recent Letter to Nature, Kraemer *et al.* [Nature (London) **440**, 315 (2006)] report on experimental “evidence for Efimov quantum states” in an ultracold gas of cesium atoms. Such quantum states refer to an infinite series of energy levels of three identical Bose particles, accumulating at the threshold for dissociation as the scattering length of each pair is tuned to infinity. Whereas the existence of a single Efimov state has been predicted for three helium atoms, earlier experimental studies concluded that this elusive state had not been found. In this paper we show by an intuitive argument and full numerical calculations that the helium and cesium experiments actually provide evidence of the same, ground state of this trimer spectrum, which the helium experimentalists and pioneering theoretical studies had not associated with Efimov’s effect. Unlike the helium trimer, the observed $^{133}\text{Cs}_3$ resonance refers to a Borromean molecular state. We discuss how as yet unobserved, excited Efimov quantum states might be detected in ultracold gases of ^{85}Rb and of ^{133}Cs at magnetic field strengths in the vicinity of 0.08 T (800 G).

PACS numbers: 34.50.-s,03.75.-b,34.10.+x,21.45.+v

I. INTRODUCTION

Efimov’s effect [1, 2, 3] refers to a scenario in which three identical Bose particles interact via weak pair potentials, each supporting only a single bound state when the s -wave scattering length a is positive. None of the pairs is bound when a is negative, while at the intersection of the two regimes the scattering length has a singularity. As early as 1935 Thomas [4] showed that under these conditions three particles can be tightly bound, despite their weak binary interactions. Thirty five years later, Efimov [1] discovered a striking extension of Thomas’ effect, predicting the existence of an infinite series of excited three-body energy levels in the limit $|a| \rightarrow \infty$. Each Efimov state emerges when a is negative at the threshold for dissociation into three free particles and vanishes eventually via decay into a two-body bound state and a third free particle as a is increased to positive values across the singularity. Such an ideal universal scaling behavior of three-particle energy levels is illustrated in Fig. 1. Two of the levels (labeled by their degree of excitation, $n = 1, 2, 3, \dots$) are visible but ideally they all have the same functional form as a is varied, the full extent of which is displayed only for the E_n level.

Strict universality in a three-body system presupposes a large scattering length whose modulus by far exceeds all the other length scales set by the pair potentials. This specific requirement on the two-particle interactions in combination with the wide spread of energy scales in Fig. 1 have for a long time prevented any generally accepted discovery of Efimov states in nature. Experimental realizations of Efimov’s scenario have been suggested, for instance, for trimer molecules consisting of three ^4He atoms [5], as well as for alkali atoms

in ultracold gases with magnetically tunable interactions (see Refs. [6, 7, 8] and references therein). Helium trimers well match the assumptions underlying Thomas’ and Efimov’s effects, as for each atom pair there exists only a single weakly bound dimer state giving rise to the large positive scattering length of about [9] $200 a_0$ (a_0 being the Bohr radius). The inter-atomic interactions are inaccessible to external manipulation but are sufficiently weak to give rise to two trimer bound states of the Thomas-Efimov spectrum.

The excited $^4\text{He}_3$ E_2 level follows the qualitative trends indicated in Fig. 1 when the pair potential is scaled to mimic a hypothetical tuning of a . In particular, it vanishes into the atom-dimer continuum as the pairwise attraction is increased [10, 11] and has therefore been referred to as a genuine Efimov state. By contrast, a rigorous variational estimate [12] reveals that the binding energy of the ground state of the Thomas-Efimov spectrum (not shown in Fig. 1) violates the global universal scaling behavior of Fig. 1, as it never intersects with the two-body level. Similar deviations from three-body universality, as $1/a$ is hypothetically increased, have been discussed in Ref. [13], in the context of the three-nucleon problem. In particular, several publications [10, 11, 14, 15] had not associated the experimentally observed [14, 15] $^4\text{He}_3$ ground state with Efimov’s effect. In the limit of zero interaction, i.e. $1/a \rightarrow -\infty$ in Fig. 1, however, this ground trimer level must vanish in a three-body zero-energy resonance.

In this paper we show that recent experiments in ultracold gases of ^{133}Cs atoms [8] also provide evidence for the ground trimer level of the Thomas-Efimov spectrum via observation of its associated zero-energy resonance. We investigate several Efimov spectra of the experimentally relevant

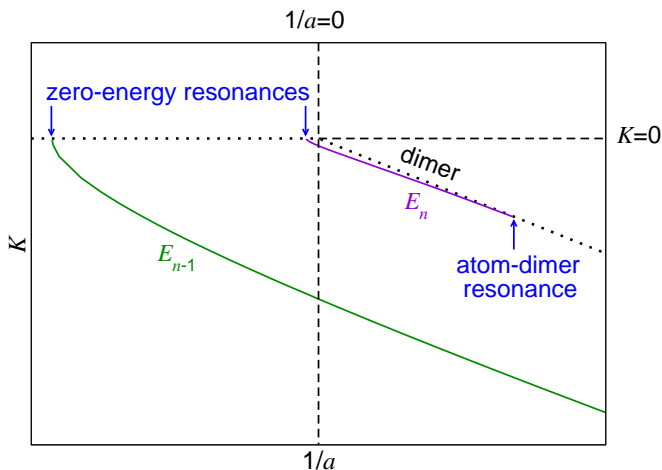


FIG. 1: (Color online) Efimov plot [1] illustrating the wave number $K = -(m|E_n|/\hbar^2)^{1/2}$ ($n = 1, 2, 3, \dots$) indicated by solid curves vs. the inverse scattering length, $1/a$. Here m is the single particle mass and E_n is the energy of the n th three-particle level. The wave number labeled dimer (dotted line) is associated with the two-body bound state emerging in the limit $1/a \rightarrow 0$ (i.e. $|a| \rightarrow \infty$) at the vertical dashed line. In accordance with Ref. [1], its energy is universal, i.e. $E_b = -\hbar^2/(ma^2)$. The limits $1/a \rightarrow \pm\infty$ of the horizontal axis refer to zeros of the scattering length. Ideally, each Efimov level emerges in a three-body zero-energy resonance at negative a and eventually vanishes into the continuum leading to an atom-dimer resonance at positive a . The ground state of the Thomas-Efimov spectrum ($n = 1$) is not displayed.

alkali atomic species ^{133}Cs and ^{85}Rb in the vicinity of singularities of the diatomic scattering length, realized by magnetically tunable Feshbach resonances [16, 17, 18]. This involves predictions of the energies of metastable trimer levels as well as numerical calculations of three-body recombination loss-rate constants [6, 7], motivated by the observations reported in Ref. [8]. Our studies indicate that ultracold gases in the presence of broad, entrance-channel dominated diatomic zero-energy resonances and negative background-scattering lengths [19] may be best suited for the detection of as yet unobserved excited trimer levels of the Thomas-Efimov spectrum [20].

The paper is organized as follows: In Section II we briefly discuss the technique of detecting three-body zero-energy resonances [6, 7, 8] in ultracold gases of ^{133}Cs at low magnetic-field strengths. Based on quantitative calculations of associated three-body recombination loss-rate constants, we interpret the measurements of Ref. [8] in terms of their relation to Efimov's effect [1, 2]. In this context, we discuss crucial shortcomings of purely universal treatments of near-resonant three-body recombination into comparatively tightly bound target-dimer states at negative as well as small positive scattering lengths [8, 21, 22]. Using an intuitive argument, we illustrate our finding that the experimentally observed three-body zero-energy resonance [8] refers to the ground state of the Thomas-Efimov spectrum. In Section III we predict magnetic-field strengths associated with excited state three-body zero-energy resonances in ultracold ^{133}Cs gases in the vicinity of 800 G.

We discuss prospects for their detection in comparison with a previous suggestion for experiments using ^{85}Rb [20]. Section IV summarizes our conclusions. Finally, the appendix provides a detailed description of our general method [23] for calculating resonance-enhanced three-body recombination loss-rate constants including the regimes of negative as well as small positive scattering lengths.

II. RESONANCE-ENHANCED THREE-BODY RECOMBINATION IN CESIUM GASES

Whereas the helium studies of Refs. [14, 15] relied upon direct observation of $^4\text{He}_3$ in a molecular beam, the existence of trimer levels in ultracold gases [8] has been inferred from three-body zero-energy resonances as illustrated in Fig. 1. Their signatures manifest themselves, for example, in a resonant enhancement of three-body recombination loss [6, 7]. In such processes three initially free atoms collide to form a dimer, while the binding energy is transferred to the relative motion of the third atom with respect to the bound pair. Their final kinetic energies are usually high enough for all three colliding particles to leave an atom trap confining an ultracold gas, whose atom number N thus decays in accordance with the rate equation

$$\dot{N} = -K_3 \langle n^2 \rangle N. \quad (1)$$

Here $\langle n^2 \rangle$ is the mean square density and K_3 is the three-body recombination loss-rate constant.

A. Ultracold collisions of cesium atoms at low magnetic-field strengths

Observation of atom loss was used in Ref. [8] to track down a three-body zero-energy resonance in gases of ^{133}Cs prepared in the ($F = 3, m_F = +3$) Zeeman ground state at temperatures ≥ 10 nK. Here F refers to the total atomic angular momentum quantum number, and m_F indicates the associated projection with respect to an applied, spatially homogeneous magnetic field of strength B . This experimental setup [8] allows magnetic tuning of the s -wave scattering length a to mimic the variation of inter-particle interactions in Efimov's scenario [1, 2], taking advantage of the occurrence of a diatomic zero-energy resonance in cesium collisions at low fields.

In the vicinity of any diatomic zero-energy resonance [24], the scattering length assumes all values between $-\infty$ and $+\infty$. The associated strong magnetic-field variation $a(B)$ can usually be described, to an excellent level of accuracy, by the following general formula [25]:

$$a(B) = a_{\text{bg}} \left(1 - \frac{\Delta B}{B - B_0} \right). \quad (2)$$

Here B_0 is the position where a has a singularity, a_{bg} is the background scattering length observed asymptotically far from B_0 , while the resonance width, ΔB , refers to the distance between B_0 and the zero-crossing point of the scattering length, i.e. $a(B_0 + \Delta B) = 0$.

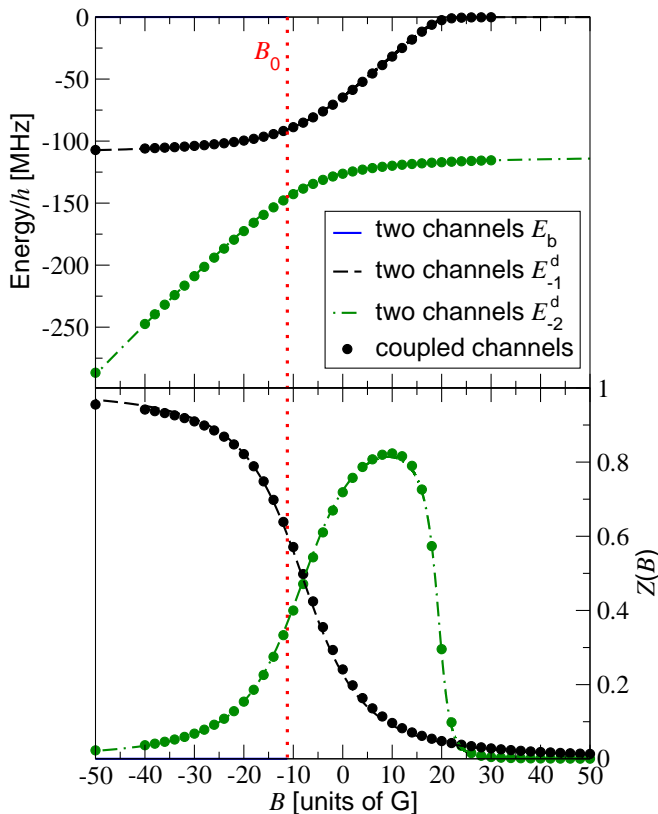


FIG. 2: (Color online) Comparison between full coupled-channels (circles) and two-channel (curves) calculations of the ^{133}Cs 6s-dimer energies (upper panel) [17, 25, 27], as well as their associated closed-channel admixtures [19], $Z(B)$ (lower panel), vs. the magnetic-field strength, B . For each magnetic-field strength zero energy is chosen to coincide with the scattering threshold. The resonance position, B_0 , is indicated by the dotted line. Curves labeled E_{-1}^d and E_{-2}^d refer to the two highest excited vibrational bound states for $B > B_0$ and the levels they adiabatically correlate with at $B < B_0$, whereas the Feshbach molecular energy E_b existing for $B < B_0$ is not resolved in the upper panel. Its closed-channel admixture in the lower panel is negligible.

In the particular case of ^{133}Cs atoms prepared in the ($F = 3, m_F = +3$) state near zero field strength, the strong B -dependence of the scattering length is driven by a diatomic zero-energy resonance in the mirror-spin-channel of atoms in the excited ($F = 3, m_F = -3$) Zeeman state. This scenario can be formally described [26] by a negative resonance position that we calculate at $B_0 = -11.2$ G ($1 \text{ G} = 10^{-4} \text{ T}$) using the complete two-body Hamiltonian model of Ref. [27], which accurately represents the positions of all known diatomic resonances in cesium collisions. An associated vibrational molecular energy spectrum is illustrated in the upper panel of Fig. 2 for isotropic 6s-dimer states [17, 25, 27], whose highest excited, Feshbach molecular, level E_b [19] (unresolved in Fig. 2) causes the zero-energy resonance at B_0 . The large, positive background-scattering length of $a_{\text{bg}} = 1720 a_0$, in combination with the resonance width of $\Delta B = 27.5$ G, allow $a(B)$ to be varied between about $-2500 a_0$ and zero within a field range between $B = 0$ and about 17 G. Beyond its zero-

crossing point the scattering length rises to a_{bg} , as shown in the inset of the upper panel of Fig. 3.

B. Three-body zero-energy resonances

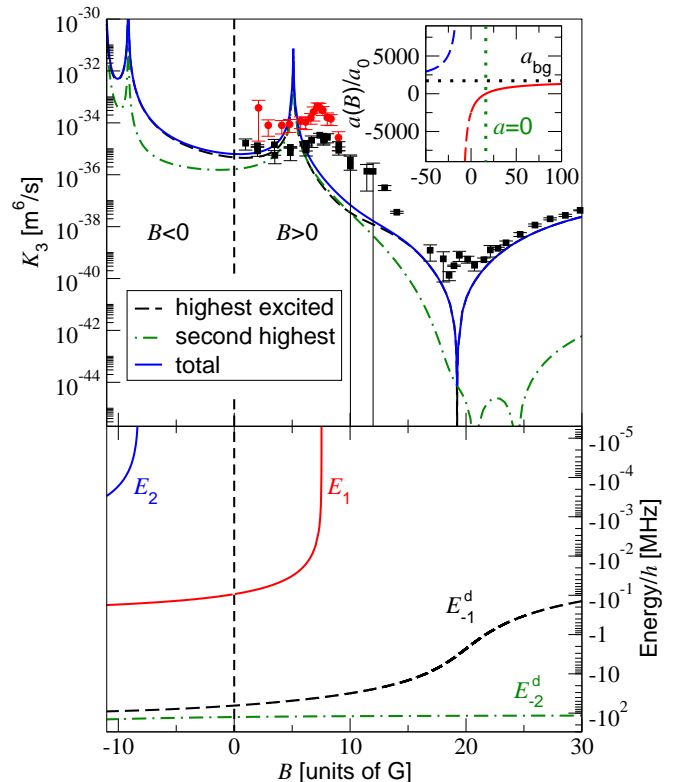


FIG. 3: (Color online) Calculated three-body recombination loss-rate constants K_3 (upper panel) and energies of metastable trimer levels of ^{133}Cs atoms labeled E_1 and E_2 (lower panel) vs. the magnetic-field strength B . For each magnetic-field strength zero energy coincides with the scattering threshold for three asymptotically free atoms. Only ranges of $B > 0$ are accessible to experiments with atoms in the Zeeman ground state, whereas $B < 0$ would be accessible to experiments with the ($F = 3, m_F = -3$) level. Measurements of K_3 [8, 28] performed at 10 nK and about 200 nK are indicated by circles and squares, respectively. The dashed and dot-dashed curves labeled E_{-1}^d and E_{-2}^d in the lower panel refer to the 6s-dimer levels [17, 25, 27] of Fig. 2, constituting the target states included in our calculations. Dashed and dot-dashed curves in the upper panel indicate their associated contributions to the total three-body recombination loss-rate constant (solid curve). The inset of the upper panel illustrates the variation of the scattering length with magnetic field.

Based on numerically exact three-body calculations without fit parameters using the method of Ref. [23], Fig. 3 shows the B -dependence of K_3 as well as the metastable $^{133}\text{Cs}_3$ level causing a three-body zero-energy resonance observed in Ref. [8] at 7.2 G. Our estimates of its position rely upon two independent methods: The first approach [20] follows Thomas' and Efimov's original treatments and accounts only for the weakly bound Feshbach molecular dimer level [19], which causes the diatomic zero-energy resonance at B_0 in the

mirror-spin-channel. This leads to a zero crossing of the energy of a trimer state at 7.5 G (solid curve labeled E_1 in Fig. 3).

Our second approach consists in directly determining the peak positions in the calculated magnetic-field dependent three-body recombination loss-rate constants [23]. In addition to the Feshbach molecule, these calculations account for the next two highest excited $6s$ -dimer levels [27] below the dimer dissociation limit, including their admixtures from different atomic Zeeman states [19], as discussed in the appendix. The associated pair potentials are based on a parametric two-channel representation of the diatomic low-energy spectra resulting solely from coupled-channels calculations. The one approximation we make in the two-body coupled-channels bound-state calculations is to neglect the relatively weak coupling of the $6s$ -levels to nearby dimer levels of predominantly d -wave symmetry. We plan future calculations in which we include such levels. Our exact solutions of the three-body Schrödinger equation have been performed at zero kinetic energy of the three initially free colliding atoms and lead to a resonance peak in K_3 at 5.1 G. We note that the second approach could also be used to calculate the Thomas-Efimov trimer levels of Fig. 3 in terms of resonant enhancements of atom-dimer collision-rate constants [23], rather than the stable bound states of the first approach. In such a more precise treatment, the atom-dimer resonances become degenerate with the zero-energy scattering threshold exactly at those magnetic-field strengths where three-body zero-energy resonances occur in the recombination loss-rate constant K_3 .

Relative to the width of the diatomic zero-energy resonance the deviations between the calculated and observed peak positions are less than 8% for both methods without any adjustments to the measured K_3 . We note that reducing the temperature of the cesium gas tends to shift the peak towards lower fields [29]. The comparison between both methods and the experiments indicates that the three-body zero-energy resonance positions in the upper panel of Fig. 3 are largely insensitive to the details of the diatomic molecular target levels. This behavior is physically sensible, as these positions depend only on the metastable Thomas-Efimov levels close to the three-body dissociation threshold in the lower panel.

C. Incompleteness of universal approaches to three-body recombination at negative scattering lengths

As opposed to universal fitting procedures [21, 22], our calculations also correctly incorporate the two- and three-body physics in the vicinity of the minimum of K_3 (just below 20 G in the upper panel of Fig. 3) and fully recover its measured position. While the overall calculated magnitudes are in good agreement with experiment throughout, we observe a strong sensitivity of K_3 to the B -dependent closed-channel admixtures [19] of the diatomic target states illustrated in the lower panel of Fig. 2. This sensitivity at negative as well as small positive scattering lengths is to be expected because the formation of a dimer from initially free atoms should be suppressed when the atoms have to change their Zeeman states during this process. These findings imply that K_3 depends on

B not only through $a(B)$ but also through the strongly varying properties of the comparatively tightly bound diatomic molecular target levels of Fig. 2. Consequently, any fit analysis of the measured data in Fig. 3 incorporating the B -dependence of K_3 only through the scattering length is incomplete, and could therefore lead to unreliable conclusions about three-body universality in the system.

D. Interpretation of the cesium experiments

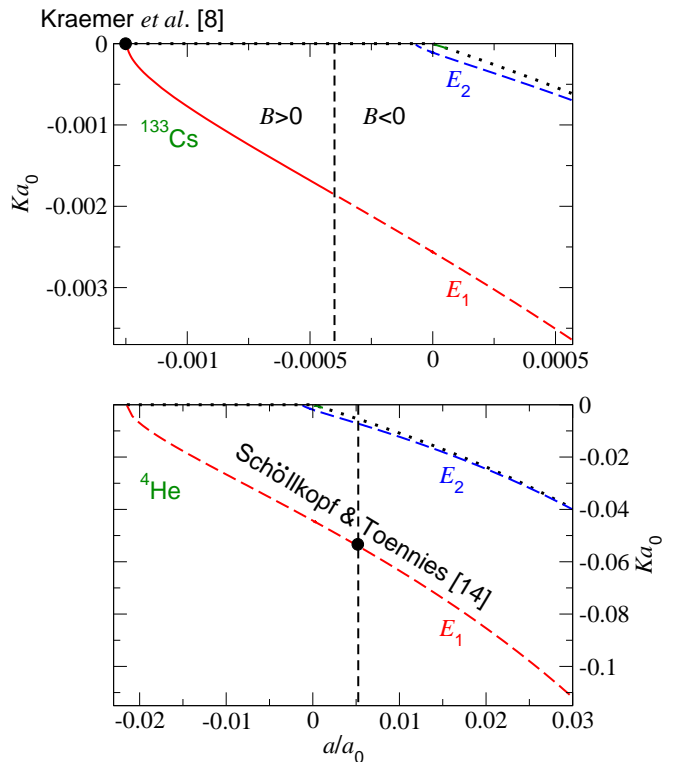


FIG. 4: (Color online) Comparison between Efimov plots associated with ^{133}Cs in the vicinity of zero field (upper panel) and ^4He (lower panel). The filled circles refer to the degree of excitation ($n = 1$) of the trimer states detected in the experiments of Refs. [8, 14] at the inverse scattering lengths indicated on the horizontal axis. Dotted curves indicate energies of dimer levels causing diatomic zero-energy resonances at $1/a = 0$. The range of scattering lengths in the upper panel extends from the observed [8] three-body zero-energy resonance position to $a = a_{\text{bg}}$ at field strengths $B < 0$. In accordance with Refs. [12, 13], the curves labeled E_1 illustrate the increasing separation of the trimer ground level from the dimer energy as $1/a$ is increased. By contrast, the E_2 level in the lower panel approaches the atom-dimer threshold. It eventually gets overrun by the dimer energy causing an atom-dimer resonance as the potential is scaled to enhance the pairwise attraction [10, 11]. For this reason, only the excited E_2 level has been referred to in Refs. [5, 10, 11, 15] as a genuine Efimov state.

Figure 3 shows that according to our calculations the resonance peak experimentally observed at 7.2 G [8] is associated with the ground trimer level of the Thomas-Efimov spectrum, E_1 . As opposed to the peak positions and magnitudes of K_3 ,

the labels attached to the trimer levels in the lower panel are independent of the detailed physics included in the approach. All that is needed for this classification is the knowledge that the observed resonance [8] is the first to appear on the low-field side of the zero crossing of the scattering length. This is immediately evident from the ^{133}Cs Efimov plot in the upper panel of Fig. 4, in which the field strength associated with $a = 0$ corresponds to the limit $1/a \rightarrow -\infty$. As B is decreased the inverse scattering length $1/a(B)$ increases. Zero magnetic-field strength is indicated by the vertical dashed line. The trimer energy spectrum beyond this point is indicated by dashed curves in the upper panel of Fig. 4 and might be accessed in gases of ^{133}Cs atoms prepared in the excited ($F = 3, m_F = -3$) Zeeman state.

For comparison, the lower panel of Fig. 4 shows the Efimov plot associated with $^4\text{He}_3$ [14, 15]. Both the cesium [8] and helium [14, 15] experiments provide evidence for the same level of the Thomas-Efimov spectrum. Whereas the $^4\text{He}_3$ molecule is stable with respect to spontaneous dissociation, the $^{133}\text{Cs}_3$ state can decay into an atom and, e.g., one of the dimer levels in the lower panel of Fig. 3 in accordance with energy conservation. We note in this context that all stable $^{133}\text{Cs}_3$ molecular levels are below the diatomic ground-state energy, whose typical modulus for alkali systems exceeds the largest $h \times 100$ MHz energy scale considered in this paper by six orders of magnitude. Consequently, the ground state of the Thomas-Efimov spectrum of cesium does not coincide with the stable molecular ground state of $^{133}\text{Cs}_3$. The resonance signature of the observed [8] metastable Thomas-Efimov cesium trimer, however, has been detected at a negative scattering length. To our knowledge, this measurement therefore provides the first experimental evidence for the existence of a Borromean [30] molecular state, i.e. a three-body energy level, with a finite width in the present context, in the absence of any diatomic levels energetically above it. Among the exotic three-atom bound molecular states of helium, including the isotope mixture $^4\text{He}_2^3\text{He}$, for instance, at least one atom pair, namely $^4\text{He}_2$, is bound [14]. Accordingly, only a “pseudo-Borromean” four-atom complex, $^4\text{He}_2^3\text{He}_2$, has been observed in molecular-beam experiments [31].

III. EXCITED THOMAS-EFIMOV TRIMER LEVELS

The prospect of an experimental verification of Efimov’s effect depends on the criterion for its discovery, since a measurement of an infinite number of trimer levels with increasingly loose bonds is impossible. Numerous pioneering studies, such as Refs. [5, 10, 11], therefore agreed that the detection of a single Efimov state would be sufficient. References [22, 32] suggest that the $^4\text{He}_3$ ground state should be referred to as the first example of an Efimov state in nature, as the modulus of the diatomic scattering length by far exceeds all the other length scales set by the pair potentials [9]. Several studies summarized in Refs. [20, 32] have shown that the $^4\text{He}_3$ molecule is indeed universal, i.e. both levels are accurately determined by the scattering length in addition to a single independent parameter [1, 22]. Such a parameter could

be provided, e.g., by recent experimental studies [15] showing that the bond lengths of the observed $^4\text{He}_3$ molecules [14] are consistent with predictions for the ground state. Several theoretical studies suggest that the ground-state triton ^3H nucleus [33] might also be described using universal treatments (see, e.g., Refs. [13, 34, 35, 36, 37]). By contrast, a recent publication [38] concludes that the discovery of the cesium three-body zero-energy resonance [8] provided the first evidence for the existence of Efimov’s effect in nature. This assessment is based on a fit analysis of the measurements universally relating the resonance position of 7.2 G to the field strength of the minimum of K_3 just below 20 G in Fig. 3. Such a procedure relies upon the assumption that universality is preserved across the zero of scattering length and that all B -dependence of $K_3(B)$ is included in $a(B)$, whereas this might be strictly justified at most in the limit $a \rightarrow +\infty$.

A. Three-body zero-energy resonances of ^{133}Cs at high field strengths in the vicinity of 800 G

Besides the existing evidence for the ground state of the Thomas-Efimov spectrum in, for instance, ^4He molecular beams and ultracold gases of ^{133}Cs , the discovery of an excited state [5, 10, 11] remains an elusive goal. Measurement of the E_2 three-body zero-energy resonance at about -9 G in Fig. 3 could provide an opportunity for such a discovery. Ultracold gases of ^{133}Cs prepared in the excited ($F = 3, m_F = -3$) Zeeman state, however, are affected by inelastic atom loss due to both two-body spin-relaxation [27, 39] and three-body recombination. Such a coincidence of loss mechanisms could lead to difficulties in the interpretation of measurements [40].

For this reason, we study three-body recombination in the vicinity of an as yet unobserved broad diatomic zero-energy resonance of ^{133}Cs gases prepared in the ($F = 3, m_F = +3$) Zeeman ground state at comparatively high magnetic-field strengths on the order of 800 G. Based on the coupled-channels model of Ref. [27] and a fit to Eq. (2), we obtain an associated singularity of the scattering length at $B_0 = 800.6$ G, as illustrated in the upper panel of Fig. 5. This fit gives the background-scattering length and resonance width to be $a_{\text{bg}} = 1918 a_0$ and $\Delta B = 83.2$ G, respectively, determining $a(B)$ via Eq. (2). Comparatively narrow zero-energy resonances at about 735 G and 825 G in Fig. 5 are neglected in this treatment.

The lower panel of Fig. 5 illustrates the complex diatomic molecular energy spectrum of ^{133}Cs in the vicinity of 800 G. Dashed curves are associated with states of predominantly d -wave symmetry, which cause the two comparatively narrow zero-energy resonances in the upper panel. Solid curves refer to the s -wave dimer levels, which are most strongly coupled to the scattering continuum above the zero-energy threshold. Among them the $6s$ -Feshbach molecular dimer state of energy E_b (not resolved in the lower panel of Fig. 5) causes the broad diatomic zero-energy resonance whose calculated position is 800.6 G. In order to give quantitative estimates for K_3 , we use the parametric two-channel representation of the s -wave dimer levels explained in the appendix, in analogy to

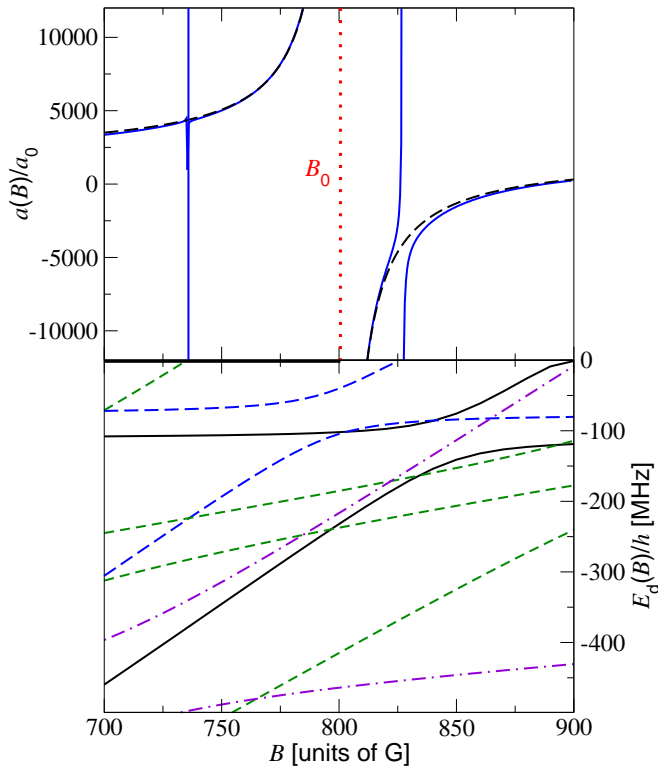


FIG. 5: (Color online) Scattering length (upper panel) and diatomic bound-state energies (lower panel) of ^{133}Cs atoms vs. magnetic-field strength in the vicinity of 800 G. The solid curve in the upper panel refers to exact coupled-channels calculations [27] including basis states of s - and d -wave symmetries, while the dashed curve is a fit of Eq. (2) to the calculated data. According to this fit, the position of the broadest singularity of the scattering length is located at $B_0 = 800.6$ G (vertical dotted line). Comparatively narrow zero-energy resonances near 735 G and 825 G are due to dimer levels of predominantly d -wave symmetry shown in the lower panel. Their energies with respect to the zero-energy dissociation threshold are indicated by long-dashed, dashed and dot-dashed curves. These states are more weakly coupled to the continuum of free atoms than s -wave dimer levels. For convenience, their mutual coupling is neglected in these calculations. Solid curves in the lower panel refer to those s -wave dimer levels that constitute the target states included in our three-body recombination calculations. The $6s$ -dimer level [27] causing the broadest singularity of the scattering length in the upper panel is unresolved on the energy scale chosen in the figure.

our treatment of three-body recombination at low magnetic fields.

Figure 6 shows calculated three-body recombination loss-rate constants as well as metastable Thomas-Efimov trimer levels causing three-body zero-energy resonances in an ultracold cesium gas at magnetic-field strengths B in the vicinity of 800 G. Similarly to Fig. 3, these predictions refer to zero kinetic energy of the three initially free colliding atoms. Based on such full calculations (upper panel of Fig. 6) as well as a simplifying single-spin-channel treatment (lower panel of Fig. 6), we estimate the three-body zero-energy resonance associated with the ground state ($n = 1$) Thomas-Efimov level to occur between 852 G and 859 G. Similarly to the results of

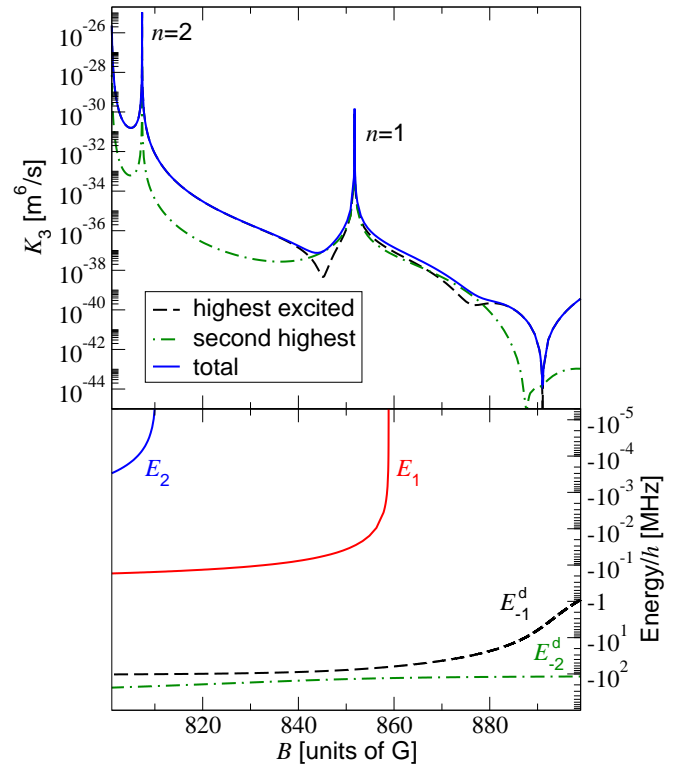


FIG. 6: (Color online) Calculated three-body recombination loss-rate constants K_3 (upper panel) and energies of metastable trimer levels of ^{133}Cs atoms labeled E_1 and E_2 (lower panel) vs. the magnetic-field strength B on the high-field side of the 800.6 G diatomic zero-energy resonance. For each magnetic-field strength zero energy in the lower panel coincides with the scattering threshold for three asymptotically free atoms. Similarly to Fig. 3, the dashed and dot-dashed curves labeled E_{-1}^d and E_{-2}^d in the lower panel refer to the s -wave dimer levels shown in the lower panel of Fig. 5, which constitute the target states included in our calculations of K_3 . Dashed and dot-dashed curves in the upper panel indicate their associated contributions to the total three-body recombination loss-rate constant (solid curve). Three-body zero-energy resonance peaks are labeled by the degree of excitation ($n = 1, 2$) of their associated metastable Thomas-Efimov trimer levels of the lower panel.

Fig. 3, the deviations between the results of these two completely different methods are less than 9% of the diatomic resonance width ΔB and mainly reflect the influence of the E_{-1}^d and E_{-2}^d dimer levels (lower panel of Fig. 6) on the three-body energy spectrum. Analogously, we estimate the position of the excited state ($n = 2$) Thomas-Efimov zero-energy resonance between 807 G and 810 G. While our calculations do not account for the full complexity of the ^{133}Cs diatomic energy spectrum, as illustrated in the lower panel of Fig. 5, we believe the accuracy of these estimates to be similar to those for the low magnetic-field strengths in Fig. 3.

In Fig. 7 we compare the total three-body recombination loss-rate constants, K_3 , associated with the low-field and high-field diatomic zero-energy resonances as functions of the scattering length, a . The overall qualitative trends of the calculated K_3 near 800 G (dashed curve) tend to be similar to those

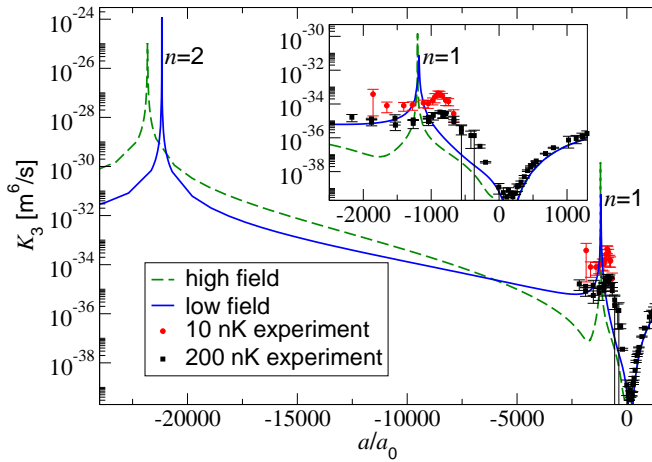


FIG. 7: (Color online) Comparison between the calculated total three-body recombination loss-rate constants K_3 associated with the low-field (solid curve) and high-field (dashed curve) diatomic zero-energy resonances of ^{133}Cs vs. the scattering length, a . Filled circles and squares refer to experimental data of Refs. [8, 28] observed at low magnetic-field strengths (see Fig. 3) in dilute gases of 10 nK and 200 nK, respectively. The range of scattering lengths displayed covers the ground-state ($n = 1$) and excited-state ($n = 2$) three-body zero-energy resonances of the Thomas-Efimov spectrum. The inset shows an enlargement of the presently experimentally accessed [8, 28] range of $a(B)$ as well as the associated calculated and measured K_3 loss-rate constants.

at low fields (solid curve). In the regime of negative scattering lengths, however, the functional dependences on a differ considerably between the two curves, demonstrating the strong sensitivity of K_3 to the different B -dependent properties of the associated, comparatively tightly bound diatomic target levels. Universal behavior of K_3 , which is insensitive to the B -dependent properties of tightly bound diatomic target states, occurs only in the limit of large, positive a , where both curves tend to agree. In this regime, three-body recombination is strongly dominated by the weakly bound, highest excited, vibrational dimer state, whose long-range wave function is determined mainly by $a(B)$ in addition to the van der Waals dispersion coefficient, C_6 [19]. These parameters also determine the positions of Thomas-Efimov three-body zero-energy resonances in our single-spin-channel estimates of their associated energy levels in the lower panels of Figs. 3 and 6 [20].

We predict a pronounced minimum of K_3 to occur at about 891 G in the vicinity of zero scattering length. According to Fig. 6, a lower estimate of the associated loss-rate constants is on the order of only 10^{-44} m⁶/s. Given the comparison between theory and experiment of Fig. 3, we believe that recombination into dimer levels beyond those included in our calculations as well as finite temperature effects could significantly increase the minimal value of K_3 . Similarly to the experiments of Refs. [41, 42], however, the associated minimal atom loss may still allow Bose-Einstein condensation of ^{133}Cs at high fields using magnetically tunable diatomic interactions. This possibility would be crucial to three-body recombination measurements at negative scattering lengths using the technique

reported in Ref. [8].

B. Thomas-Efimov spectrum of ^{85}Rb

Both examples of diatomic zero-energy resonances of ^{133}Cs discussed in this paper were broad and entrance-channel dominated [19]. Entrance-channel dominance allowed us to describe and interpret near threshold three-atom resonance states using single-spin-channel models, largely in accordance with Thomas' [4] and Efimov's [1] original treatments. Their broad nature should be crucial for a possible experimental resolution of several three-body zero-energy resonances, given present limitations in magnetic-field control. In both of these examples, however, the background-scattering length was positive. This implies that the dominant three-body recombination peak refers to the previously observed ground state of the Thomas-Efimov spectrum, whereas the excited-state peaks occur at large negative scattering lengths ($|a| > 20000 a_0$ in Fig. 7) and accordingly large K_3 loss-rate constants. Consequently, fast depletion of an ultracold gas at such near resonant magnetic-field strengths as well as thermal broadening of peaks [43] could impose limitations on the feasibility of associated measurements. Recent studies [44] therefore suggest alternative measurements in mixtures of ultracold gases with unequal masses of the constituent particles. In such systems the number of exotic three-body energy levels depends sensitively on the associated mass ratios (see Refs. [45, 46] and references therein).

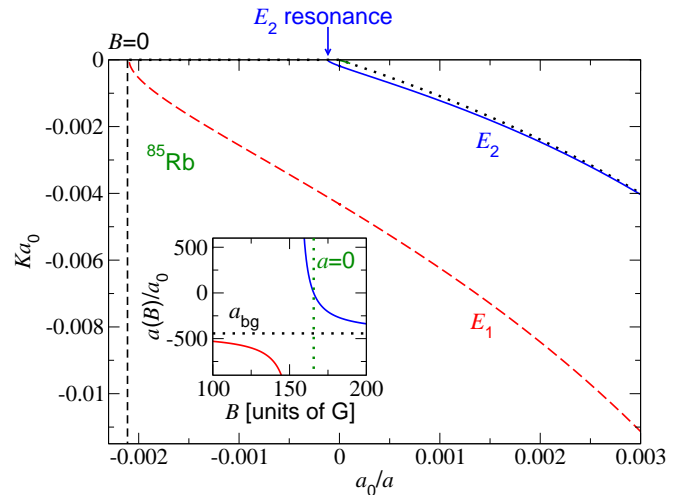


FIG. 8: (Color online) Efimov plot associated with ^{85}Rb trimers [20] in the vicinity of the 155 G diatomic zero-energy resonance. The solid and dashed curves refer to the E_2 and E_1 levels, respectively, while the dotted line indicates the energy of the Feshbach molecular dimer state. The inset shows the magnetic-field dependence of the scattering length $a(B)$ for this atomic species with a negative background-scattering length of $a_{\text{bg}} = -443 a_0$ [47].

In accordance with Ref. [20], ultracold gases with broad, entrance-channel dominated diatomic zero-energy resonances [19] and negative background-scattering lengths may be best

suites for the observation of an excited trimer state in the original context of Efimov's suggestion for identical Bose particles of equal mass [1]. An associated Efimov plot is shown in Fig. 8 for the example of ^{85}Rb in the vicinity of 155 G. According to the inset, the inverse scattering length $1/a(B)$ increases with increasing B and extends from zero field (dashed vertical line) to the zero of the scattering length at about 165.71 G [47, 48]. Consequently, a range of $1/a$ from $1/a_{\text{bg}} < 0$ to $+\infty$ is experimentally accessible. As opposed to the cesium case in the upper panel of Fig. 4, the ground Thomas-Efimov level never reaches the threshold in the vicinity of $B_0 = 155$ G. Consequently, the only available three-body zero-energy resonance refers to the excited and as yet unobserved E_2 level.

Besides the possibility of measuring an associated three-body recombination loss-rate peak, the existence of the excited Thomas-Efimov state could be verified by populating this trimer level using a magnetic-field sweep technique [20]. Such experiments might be performed in the gas phase as well as in optical lattices with three atoms occupying each site [20, 49, 50, 51]. Due to the larger spatial extents of their bound-state wave functions [20], the lifetimes of excited E_2 states of $^{85}\text{Rb}_3$, with respect to spontaneous dissociation via either spin relaxation [48, 52] or atom-dimer relaxation [53, 54], should be significantly longer than those of ground states of the Thomas-Efimov spectrum. Such an increase in lifetime of these ultracold trimer molecules might be sufficient for experimental studies of their exotic properties.

IV. CONCLUSIONS

We have shown by an intuitive argument as well as full numerical calculations that the recent observation of a three-body zero-energy resonance in ultracold ^{133}Cs gases [8] refers to the ground level of the Thomas-Efimov spectrum that has been discovered in ^4He molecular-beam experiments [14]. Unlike $^4\text{He}_3$, the metastable cesium trimer observed in the experiments of Ref. [8] is associated with a Borromean state [30], providing, to our knowledge, the first experimental evidence for their existence in molecular physics. Our studies show that resonance-enhanced three-body recombination in ultracold gases at negative as well as small positive scattering lengths is sensitive to the strongly magnetic-field dependent Zeeman-state compositions of the comparatively tightly bound diatomic target states. This implies that fitting procedures incorporating the magnetic-field dependence of the rate constants only through the scattering length are incomplete and could therefore lead to unreliable conclusions about universality of trimer levels. As opposed to the magnitudes of the loss-rate constants, the mere magnetic-field positions of Thomas-Efimov zero-energy resonances largely follow the qualitative trends implied by three-body universality, irrespective of the details of diatomic energy levels far away from the scattering threshold.

The long-standing problem of detecting excited Thomas-Efimov states [10, 11, 15] remains an elusive goal. Based on numerical predictions of three-body recombination loss-

rate constants, we have investigated the possibility of observing associated three-body zero-energy resonances in ultracold ^{133}Cs gases. Our studies focused on a broad, entrance-channel dominated [19] diatomic zero-energy resonance, which is predicted to occur near 800 G. In this case, the background-scattering length is positive. We have shown that for this reason an associated experiment would require observation of two distinct three-body recombination loss-rate peaks. The excited state three-body zero-energy resonance occurs at large negative scattering lengths. Thermal broadening [43] as well as strong atom loss could therefore impose limitations on the feasibility of associated measurements. We reach the conclusion that ultracold gases involving entrance-channel dominated diatomic zero-energy resonances with negative background-scattering lengths, such as ^{85}Rb , may be best suited for the first observation of excited Thomas-Efimov trimers. Their detection might be achieved by populating such metastable states, with sufficient lifetimes, via magnetic-field sweeps [20] in ultracold gases or in optical lattices with three atoms occupying each site [20, 49, 50, 51].

V. ACKNOWLEDGMENTS

We are grateful to Tobias Kraemer for providing measured data sets of Refs. [8, 28] to us, as well as to Vitaly Efimov for his advice on signatures of universal three-body states in nature, especially with regard to the three-nucleon problem. We thank Françoise Masnou-Seeuws, Francesca Ferlaino, Hanns-Christoph Nägerl, Rudolf Grimm, José D'Incao, Brett Esry, Chris Greene, Wieland Schöllkopf, and Peter Toennies for many helpful discussions. This research has been supported by the Royal Society and the UK EPSRC.

APPENDIX A: AGS APPROACH TO THREE-BODY RECOMBINATION

1. Scattering matrix

a. Asymptotic scattering channels

Throughout this appendix, we consider collisions between three identical Bose atoms. Three-body scattering is characterized by the arrangements of the atoms on asymptotically large time scales before and after a collision. These arrangements determine the asymptotic entrance- and exit-scattering channels. Such channels can involve a bound molecular pair of atoms asymptotically spatially separated from the third atom or three free atoms. In the case of three-body recombination the entrance channel consists of three asymptotically free atoms, whereas the exit channel contains a diatomic molecule and a free atom.

To characterize the positions of the atoms in the different asymptotic scattering channels, we choose the Jacobi coordinates of Fig. 9 in the center-of-mass frame. These coordinates are particularly well suited to describe asymptotic arrangements involving a bound pair and a free atom. In the

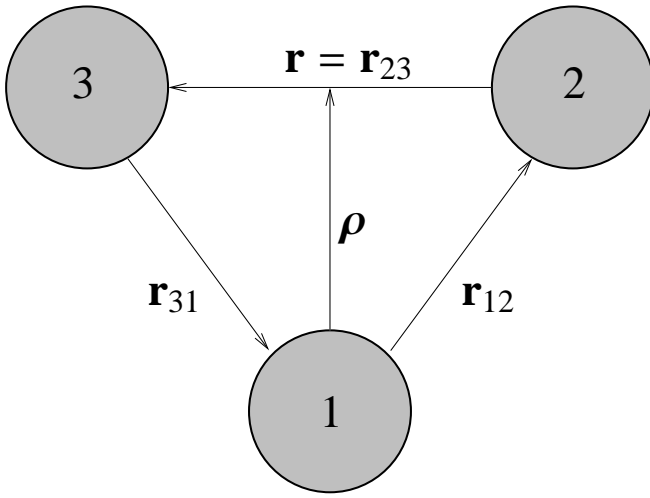


FIG. 9: Jacobi coordinates of the relative motion of three atoms. The set of coordinates $\boldsymbol{\rho} = \boldsymbol{\rho}_1$ and $\mathbf{r} = \mathbf{r}_1$ is selected in such a way that it describes the hypothetical situation of an interacting pair of atoms (2, 3), whereas atom 1 is considered as a spectator. Two other sets of these coordinates describing different arrangements of the atoms can be obtained through cyclic permutations of the atomic indices.

following, we label the sets of coordinates by the Greek index $\alpha = 1, 2, 3$ of the free atom. For convenience, the particular set of coordinates shown in Fig. 9 will be denoted, without explicit reference to its index, simply by $(\boldsymbol{\rho}, \mathbf{r})$.

b. Transition matrices

We assume the three atoms to interact pairwise depending on their internal Zeeman states [23]. Consequently, the three-body Hamiltonian in the barycentric frame,

$$H = H_0 + V_1 + V_2 + V_3, \quad (\text{A1})$$

is comprised of a kinetic energy contribution,

$$H_0 = |\text{bg}\rangle \left[-\frac{\hbar^2}{2(\frac{2}{3}m)} \nabla_{\boldsymbol{\rho}}^2 - \frac{\hbar^2}{2(\frac{m}{2})} \nabla_{\mathbf{r}}^2 \right] \langle \text{bg}|, \quad (\text{A2})$$

in addition to the pair potentials V_1 , V_2 , and V_3 . Here m is the atomic mass, $|\text{bg}\rangle$ denotes the entrance-channel spin product state, consisting of the three one-body Zeeman states in which the atoms of the gas are prepared, and V_1 is the potential of the atom pair (2, 3). The remaining interactions V_2 and V_3 are determined through cyclic permutations of the atomic indices. Each potential couples entrance- and closed-channel Zeeman state configurations in Feshbach resonance-enhanced collisions [23]. As the entire physics described in this paper involves energy ranges in the close vicinity of the scattering threshold, and accordingly large interparticle distances, we have neglected short-ranged, genuinely three-body forces in our approach [11, 55].

The probabilities for transitions between the different asymptotic scattering channels can be conveniently described

in terms of the scattering matrix S . To determine the S -matrix, we follow the approach by Alt, Grassberger and Sandhas (AGS) [56, 57] and introduce the following Green's functions associated with the different asymptotic arrangements of the atoms:

$$G_0(z) = (z - H_0)^{-1}, \quad (\text{A3})$$

$$G_{\alpha}(z) = (z - H_0 - V_{\alpha})^{-1}. \quad (\text{A4})$$

Here z is a complex variable with the dimension of an energy. Throughout this appendix this variable is given by a limit, $z = E_i + i0$, indicating that the energy of the three initially noninteracting atoms, E_i , is approached from the upper half of the complex plane. The free Green's function $G_0(z)$ is associated with three asymptotically free atoms, while $G_{\alpha}(z)$ describes the configuration in which the atom with the index α is free and the remaining atom pair interacts via the potential V_{α} . The complete Green's function

$$G(z) = (z - H)^{-1} \quad (\text{A5})$$

implicitly determines the AGS transition matrix $U_{\alpha\beta}(z)$ through the relation:

$$G(z) = \delta_{\alpha\beta} G_{\beta}(z) + G_{\alpha}(z) U_{\alpha\beta}(z) G_{\beta}(z). \quad (\text{A6})$$

Here the indices $\beta = 0$ and $\alpha = 0$ are associated with entrance and exit channels involving three free atoms, respectively. The indices $\beta, \alpha = 1, 2, 3$ correspond to arrangements in which the atom with the index β or α is free, respectively, while the remaining atom pair is bound to a molecule.

The transition matrices $U_{\alpha\beta}(z)$ determine the elements of the S -matrix associated with the different asymptotic scattering channels. The general derivations of Refs. [56, 57] show, in particular, that the S -matrix element for three-body recombination into a diatomic molecular bound state $|\phi_d\rangle$ is given by the formula:

$$\begin{aligned} {}_{\alpha} \langle \mathbf{q}_f, \phi_d | S | \mathbf{q}_i, \mathbf{p}_i, \text{bg} \rangle &= -2\pi i \delta(E_f - E_i) \\ &\times {}_{\alpha} \langle \mathbf{q}_f, \phi_d | U_{\alpha 0}(z) | \mathbf{q}_i, \mathbf{p}_i, \text{bg} \rangle. \end{aligned} \quad (\text{A7})$$

Here $|\mathbf{q}_i, \mathbf{p}_i, \text{bg}\rangle = |\mathbf{q}_i\rangle |\mathbf{p}_i\rangle |\text{bg}\rangle$ and $|\mathbf{q}_f, \phi_d\rangle_{\alpha} = |\mathbf{q}_f\rangle_{\alpha} |\phi_d\rangle_{\alpha}$ are the general unsymmetrized initial and final momentum-normalized energy states associated with the entrance and exit channels, respectively. Consequently, \mathbf{p} and \mathbf{q} denote the momenta associated with the Jacobi coordinates \mathbf{r} and $\boldsymbol{\rho}$, respectively. This implies, for instance, that \mathbf{q}_f is the momentum of the center of mass of the molecule produced relative to the free atom with index α , and $\langle \boldsymbol{\rho} | \mathbf{q}_f \rangle = \exp(i \mathbf{q}_f \cdot \boldsymbol{\rho} / \hbar) / (2\pi\hbar)^{3/2}$ is the associated plane wave. Similarly, $|\phi_d\rangle_{\alpha}$ is the diatomic molecular state of the interacting atom pair in the exit channel. We have arbitrarily chosen the Jacobi momenta describing the entrance-channel state in accordance with the selection of atom 1 in Fig. 9 and omitted the index associated with this particular arrangement of particles. The asymptotic energies of the three atoms in the barycentric frame are symmetric with respect to permutations of particles and related to the Jacobi

momenta by the formulae:

$$E_i = \frac{3q_i^2}{4m} + \frac{p_i^2}{m}, \quad (\text{A8})$$

$$E_f = \frac{3q_f^2}{4m} + E_d. \quad (\text{A9})$$

Here E_d is the binding energy associated with the diatomic molecular target state $|\phi_d\rangle_\alpha$. Consequently, the entrance- and exit-channel states solve the Schrödinger equations $H_0|\mathbf{q}_i, \mathbf{p}_i, \text{bg}\rangle = E_i|\mathbf{q}_i, \mathbf{p}_i, \text{bg}\rangle$ and $(H_0 + V_\alpha)|\mathbf{q}_f, \phi_d\rangle_\alpha = E_f|\mathbf{q}_f, \phi_d\rangle_\alpha$, respectively. The S -matrix elements for transitions between other scattering channels can be represented in terms of the transition matrices of Eq. (A6) through formulae similar to Eq. (A7) [56, 57].

2. Three-body recombination loss-rate constant

a. Probability for the recombination of three atoms

To determine the three-body recombination loss-rate constant, we consider three initially free atoms in a large box of volume \mathcal{V} which will later be taken to be infinite. The probability P_{fi} for recombination into the molecular bound state $|\phi_d\rangle$, in a time interval of length Δt , can be obtained using Fermi's golden rule. This yields:

$$P_{\text{fi}} = \frac{18 (2\pi\hbar)^6}{\hbar^2 \mathcal{V}^2} \int d\mathbf{q}_f \left(\frac{\sin \left[\frac{1}{2}(E_f - E_i)\Delta t/\hbar \right]}{\frac{1}{2}(E_f - E_i)/\hbar} \right)^2 \times \left| {}_1\langle \mathbf{q}_f, \phi_d | U_{1,0}(z) \mathcal{S} | \mathbf{q}_i, \mathbf{p}_i, \text{bg} \rangle \right|^2. \quad (\text{A10})$$

We note that the complex argument “ $z = E_i + i0$ ” of the transition matrix $U_{1,0}(z)$ indicates that the physical energy E_i is approached from the upper half of the complex plane. To account for the identical nature of the Bose atoms, the entrance-channel state $|\mathbf{q}_i, \mathbf{p}_i, \text{bg}\rangle_1 (2\pi\hbar)^3/\mathcal{V}$ in Eq. (A10) is symmetrized by the projection

$$\mathcal{S} = \frac{1}{6} \sum_{\mathcal{P} \in \mathcal{S}_3} \mathcal{P}, \quad (\text{A11})$$

where the sum extends over all $3! = 6$ permutations \mathcal{P} of the atoms. Due to the symmetric nature of the projected initial wave function in Eq. (A10) the index $\alpha = 1$ associated with the final atomic arrangement is arbitrary.

The approximations underlying the Fermi golden rule argument and the associated continuum limit of the energy states of the box determine the range of validity of Eq. (A10). The time scale Δt is limited from above by the requirement that phenomena associated with secondary collisions of atoms due to reflection from the boundaries of the box are negligible. This implies that Δt must be much smaller than the ground-state period of the box. This gives the restriction

$$\Delta t \ll \hbar/E_g^{\text{box}} = 2m\mathcal{V}^{2/3}/(\pi^2\hbar), \quad (\text{A12})$$

where $E_g^{\text{box}} = \hbar^2\pi^2/(2m\mathcal{V}^{2/3})$ is the single-particle ground-state energy of the box. Given that ultracold collision energies E_i are usually far below the breakup threshold, i.e. $E_i \ll |E_d|$, a simple calculation using Eqs. (A8) and (A9) shows that the condition

$$\hbar/|E_d| \ll \Delta t \quad (\text{A13})$$

allows us to perform the formal limit

$$\left(\frac{\sin \left[\frac{1}{2}(E_f - E_i)\Delta t/\hbar \right]}{\frac{1}{2}(E_f - E_i)/\hbar} \right)^2 \Big|_{\Delta t \rightarrow \infty} \sim 2\pi\hbar\delta(E_f - E_i)\Delta t \quad (\text{A14})$$

in the integral over the final momentum \mathbf{q}_f of Eq. (A10). The applicability of Eq. (A14) ensures that the transition probability per unit time, i.e. $P_{\text{fi}}/\Delta t$, is independent of Δt within the limitations set by Eqs. (A12) and (A13). We note that the lower bound on Δt set by Eq. (A13) is also necessary for the validity of Eq. (A10). The time scale $\hbar/|E_d|$ is therefore characteristic for a three-body recombination event.

b. Three-body recombination loss rate for a thermal Bose gas

The interpretation of atom loss observed in a dilute atomic gas in terms of rate phenomena associated with any chemical reaction crucially relies upon the possibility of introducing coarse-grained scales in space and time. To this end, we divide the volume of the gas into regions of virtually constant density $n(\mathbf{x})$ characterized by their central position \mathbf{x} . The volume \mathcal{V} of each region sets the scale for the unit of length in the coarse-graining approach. The unit of time Δt is limited by Eqs. (A12) and (A13) except that the volume of the box in Eq. (A12) needs to be replaced by $[n(\mathbf{x})]^{-1}$. This replacement rules out collisions of three specific colliding atoms with any other constituents of the gas during a time interval of length Δt . Equations (A12) and (A13) thus determine the condition for the applicability of a rate treatment of three-body recombination in a dilute gas to be:

$$|E_d| \gg [n(\mathbf{x})]^{2/3}\hbar^2/m. \quad (\text{A15})$$

In the absence of diatomic zero-energy resonances Eq. (A15) is fulfilled for most realistic sets of physical parameters of dilute ultracold gases. Magnetic tuning of the bound-state energy E_b of the highest excited vibrational state, however, may violate this condition.

Given that Eq. (A15) applies, we follow the treatment of Ref. [58] to derive the loss-rate constant for three-body recombination. This treatment relies upon a summation of the microscopic transition probabilities of Eq. (A10), per unit time Δt , over the number $\binom{N}{3} \approx N^3/6$ of atomic triplets in a region with N atoms. This yields the number of recombination events. Under the assumption that all three atoms are lost in each recombination event, the associated loss-rate constant in a thermal ultracold Bose gas is given by the formula:

$$\begin{aligned} K_3 &= \frac{1}{2} \mathcal{V}^2 P_{\text{fi}}/\Delta t \\ &= \frac{12\pi m}{\hbar} (2\pi\hbar)^6 q_f \int d\Omega_f \left| {}_1\langle \mathbf{q}_f, \phi_d | U_{1,0}(z) | 0 \rangle \right|^2. \end{aligned} \quad (\text{A16})$$

Here $d\Omega_f$ denotes the angular component of $d\mathbf{q}_f$. In the derivation of Eq. (A16) we have taken advantage of the fact that the transition amplitude ${}_1\langle\mathbf{q}_f, \phi_d|U_{1,0}(E_i + i0)S|\mathbf{q}_i, \mathbf{p}_i, \text{bg}\rangle$ of Eq. (A10) is often insensitive with respect to typical collision energies E_i of a cold gas. For convenience, we have thus approximated the entrance-channel state by the zero-momentum plane wave $|0\rangle$ of the relative motion of three noninteracting entrance-channel atoms and performed the limit $z = i0$. The energy conservation implied by Eq. (A14) then determines the modulus of the final momentum of the diatomic molecule relative to the third, free, atom to be:

$$q_f = 2\sqrt{m|E_d|/3}. \quad (\text{A17})$$

The rate equation for the total number of atoms in a cold gas, $N(t)$, can be obtained through averaging the local rate equations over all regions of constant density. This local density approach yields Eq. (1). If recombination events occur in a Bose-Einstein condensate then the three-body recombination rate $K_3\langle n^2(t)\rangle$ needs to be divided by a factor of $3! = 6$ [59, 60], because the zero-energy entrance-channel state $|0\rangle$ is already symmetric with respect to permutations of atoms [58].

3. AGS method

a. AGS equations for transition matrices

In the following, we describe the general approach we have employed to determine the transition amplitude of Eq. (A16) based on the AGS method [56, 57]. Other techniques for solving the three-body Schrödinger equation in the context of ultracold collisions often rely upon hyperspherical-coordinate representations (see, e.g., Refs. [6, 7, 61, 62, 63]). According to Refs. [56, 57], all complete transition matrices fulfill the coupled AGS equations:

$$U_{\alpha\beta}(z) = (1 - \delta_{\alpha\beta})G_0^{-1}(z) + \sum_{\substack{\gamma=1 \\ \gamma \neq \beta}}^3 U_{\alpha\gamma}(z)G_\gamma(z)V_\gamma, \quad (\text{A18})$$

$$U_{\alpha\beta}(z) = (1 - \delta_{\alpha\beta})G_0^{-1}(z) + \sum_{\substack{\gamma=1 \\ \gamma \neq \alpha}}^3 V_\gamma G_\gamma(z)U_{\gamma\beta}(z). \quad (\text{A19})$$

Here both Eq. (A18) and Eq. (A19) determine the transition matrices $U_{\alpha\beta}(z)$ with indices $\alpha, \beta = 1, 2, 3$. We shall refer to them as the prior and post versions of the AGS equations, respectively. Given the solution to these equations we insert $\beta = 0$ into the prior version of Eq. (A18). This yields:

$$U_{\alpha 0}(z) = G_0^{-1}(z) + \sum_{\gamma=1}^3 U_{\alpha\gamma}(z)G_\gamma(z)V_\gamma. \quad (\text{A20})$$

Taking advantage of the invariance of the zero-energy plane-wave state with respect to permutations of the atoms, the AGS equation (A20) gives the transition amplitude of Eq. (A16) to

be:

$$\begin{aligned} {}_1\langle\mathbf{q}_f, \phi_d|U_{1,0}(z)|0\rangle &= \sum_{\beta=1}^3 {}_1\langle\mathbf{q}_f, \phi_d|U_{1\beta}(z)G_\beta(z)V_\beta|0\rangle \\ &= \sum_{\alpha=1}^3 {}_\alpha\langle\mathbf{q}_f, \phi_d|U_{\alpha 1}(z)G_1(z)V_1|0\rangle. \end{aligned} \quad (\text{A21})$$

We note that each transition matrix $U_{\alpha\beta}(z)$ is equivalent to the complete three-body Green's function due to Eq. (A6). The solutions of the coupled sets of equations (A18) as well as (A19) thus determine all energy levels of the three-body Hamiltonian rather than just the transition amplitudes between asymptotic channel states.

b. AGS equations for the three-body recombination transition amplitude

To render the problem of determining the exact amplitude of Eq. (A21) into a more practical form, we introduce the following wave functions:

$$|\psi_{\alpha 1}\rangle = U_{\alpha 1}(z)G_1(z)V_1|0\rangle, \quad (\text{A22})$$

$$|\psi_{\alpha 1}^i\rangle = G_0^{-1}(z)G_1(z)V_1|0\rangle(1 - \delta_{\alpha 1}). \quad (\text{A23})$$

Here the index α assumes the values $\alpha = 1, 2, 3$. A straightforward calculation using Eq. (A19) shows that $|\psi_{\alpha 1}\rangle$ is determined by the coupled set of Faddeev-type [64] equations:

$$|\psi_{\alpha 1}\rangle = |\psi_{\alpha 1}^i\rangle + \sum_{\substack{\gamma=1 \\ \gamma \neq \alpha}}^3 V_\gamma G_\gamma(z)|\psi_{\gamma 1}\rangle. \quad (\text{A24})$$

The solution of Eq. (A24) gives the transition amplitude for three-body recombination to be:

$${}_1\langle\mathbf{q}_f, \phi_d|U_{1,0}(z)|0\rangle = \sum_{\alpha=1}^3 {}_\alpha\langle\mathbf{q}_f, \phi_d|\psi_{\alpha 1}\rangle. \quad (\text{A25})$$

We use Eq. (A24) to determine the associated loss-rate constant of Eq. (A16), the implementation of which we discuss in Subsection A 5. In the following subsection, we first provide a detailed description of the interatomic potentials.

4. Resonance-enhanced three-body recombination

a. Three-body spin channels

Ultracold resonance-enhanced diatomic interactions [16, 17, 19] usually occur due to coupling between the entrance-spin-channel and a single energetically closed channel. For all the broad diatomic zero-energy resonances described in this paper the physical origin of this coupling is predominantly spin exchange [17, 65]. In the context of three-body collisions the resonant closed channel is characterized by a Zeeman-state configuration, $|\text{cl}\rangle_\alpha$. Here the index $\alpha = 1, 2, 3$ indicates

that atom α is in the Zeeman state in which the Bose gas is prepared, whereas the remnant atom pair is in the closed-channel spin state, whose strong coupling to the entrance channel causes a diatomic zero-energy resonance [16, 17, 19]. The three-body spin state is orthogonal to the product state $|\text{bg}\rangle$, i.e. ${}_{\alpha}\langle\text{cl}|\text{bg}\rangle = 0$. In the case of, e.g., the ^{133}Cs low-field zero-energy resonance of Figs. 2 and 3 the resonant diatomic closed channel is comprised of Zeeman states mainly from the upper $F = 4$ hyperfine level, whereas the atoms are prepared in the $(F = 3, m_F = 3)$ Zeeman ground state. This implies the orthogonality relation,

$${}_{\alpha}\langle\text{cl}|\text{cl}\rangle_{\beta} = \delta_{\alpha\beta}, \quad (\text{A26})$$

for all indices $\alpha, \beta = 1, 2, 3$ of the three-body closed-channel spin states. We assume in the following that the resonant inter-channel coupling fulfills Eq. (A26), i.e. no single-atom Zeeman state is shared between the diatomic entrance and closed channels. This assumption does not affect our description of diatomic energy levels for which the closed channel is always orthogonal to the entrance-spin-channel, even when single-particle Zeeman states are shared between them. It facilitates, however, our calculations of three-body recombination loss-rate constants in ^{133}Cs gases and is strictly valid only for the low-field resonance shown in Figs. 2 and 3.

b. Single-resonance approach

Resonant enhancement of ultracold collisions is often well described in terms of near degeneracy of a single diatomic closed-channel energy state, $|\phi_{\text{res}}\rangle$, with the dissociation threshold of the entrance channel [16, 17, 19]. In an extension of this concept to three-body scattering the resonance state, $|\phi_{\text{res}}, \text{cl}\rangle_{\alpha}$, refers to the situation in which a pair of atoms occupies the state $|\phi_{\text{res}}\rangle$, whereas the third atom with index α plays the role of a spectator. Throughout this appendix we choose $|\phi_{\text{res}}\rangle$ to be unit normalized, i.e. $\langle\phi_{\text{res}}|\phi_{\text{res}}\rangle = 1$. In accordance with such a single-resonance approach, the pair potentials of the three-body Hamiltonian (A1) are of the following general form [23]:

$$\begin{aligned} V_{\alpha} = & |\text{bg}\rangle V_{\alpha}^{\text{bg}} \langle\text{bg}| + |\phi_{\text{res}}, \text{cl}\rangle_{\alpha} E_{\text{res}}(B) {}_{\alpha}\langle\phi_{\text{res}}, \text{cl}| \\ & + W_{\alpha} |\phi_{\text{res}}, \text{bg}\rangle_{\alpha} {}_{\alpha}\langle\phi_{\text{res}}, \text{cl}| \\ & + |\phi_{\text{res}}, \text{cl}\rangle_{\alpha} {}_{\alpha}\langle\phi_{\text{res}}, \text{bg}| W_{\alpha}. \end{aligned} \quad (\text{A27})$$

Here V_{α}^{bg} is the background-scattering potential, $W_{\alpha}(\mathbf{r}_{\alpha})$ is the potential energy of interchannel coupling depending on the relative position \mathbf{r}_{α} of atoms of an interacting pair, and $E_{\text{res}}(B)$ is the resonance-state energy [19]. As we have chosen zero energy to coincide with the scattering threshold for three asymptotically free atoms, the three-body Hamiltonian (A1) depends on the magnetic-field strength only through $E_{\text{res}}(B)$. To a good approximation this dependence is determined by [25]:

$$E_{\text{res}}(B) = \mu_{\text{res}}(B - B_{\text{res}}). \quad (\text{A28})$$

Here μ_{res} is the difference in magnetic moment of the resonance state and a pair of asymptotically separated entrance-channel atoms, and B_{res} is the crossing point between E_{res} and

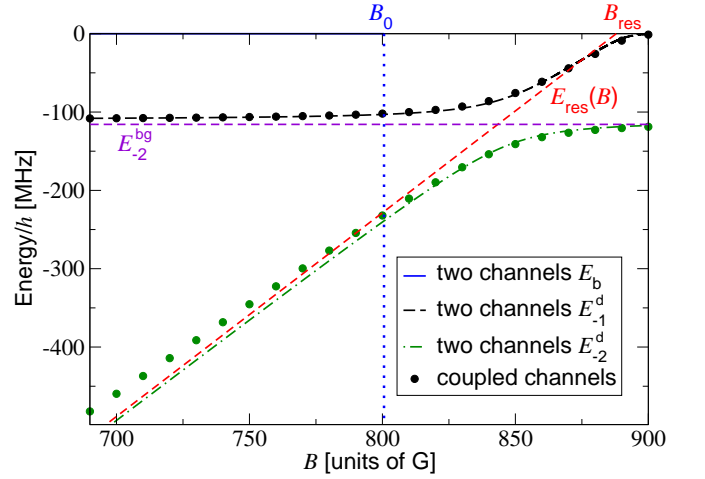


FIG. 10: (Color online) Comparison between coupled-channels (filled circles) and two-channel single-resonance (long-dashed and dot-dashed curves) approaches to the highest excited vibrational s -wave states of $^{133}\text{Cs}_2$ vs. the magnetic-field strength B in the vicinity of 800 G. The dashed line labeled $E_{\text{res}}(B)$ indicates the bare Feshbach resonance-state energy, while the horizontal dashed line refers to the second highest excited bare vibrational level of the background-scattering potential, E_{-2}^{bg} . The energies of the associated highest excited bare level, E_{-1}^{bg} , and of the Feshbach molecular dimer state, $E_b(B)$, are not resolved. The point of degeneracy of E_b with the scattering threshold (zero energy) is indicated by the vertical dotted line labeled B_0 . It coincides with the position of the broad singularity of the scattering length in Fig. 5. This measurable zero-energy resonance position is distinct from the zero-energy crossing point of the bare Feshbach-resonance level, B_{res} . The deviation at lower B -fields between the coupled-channels and two-channel E_{-2}^{d} levels is mainly due to a strong avoided crossing of dressed, coupled-channels s -states in the vicinity of 600 G, which is not included in the two-channel approach.

the entrance-channel scattering threshold, i.e. $E_{\text{res}}(B_{\text{res}}) = 0$. Figure 10 shows that for the entrance-channel dominated diatomic zero-energy resonances [19] studied in this paper, B_{res} is considerably shifted with respect to the measurable position B_0 of the singularity of $a(B)$ referred to in Eq. (2).

5. Implementation of the AGS equations

a. Interchannel coupling

For convenience, the contributions to Eq. (A27) describing interchannel coupling can always be represented in terms of an amplitude ζ , and a wave function $|\chi\rangle$, i.e.

$$W|\phi_{\text{res}}\rangle = |\chi\rangle\zeta. \quad (\text{A29})$$

Within a limited range of energies close to the dissociation threshold the precise functional form of $\chi(r) = \langle\mathbf{r}|\chi\rangle$, associated with its dependence on the distance $r = |\mathbf{r}|$ between atoms of an interacting pair, is unresolved. As a consequence, several different models of coupling are capable of predicting the same low-energy physics. For this reason, it is sufficient

for all applications in this paper to describe the interchannel coupling simply in terms of an amplitude and a range. In accordance with Ref. [66], we choose the following arbitrary but convenient Gaussian function in momentum space:

$$\chi(p) = \langle \mathbf{p} | \chi \rangle = \frac{e^{-p^2 \sigma^2 / (2\hbar^2)}}{(2\pi\hbar)^{3/2}}. \quad (\text{A30})$$

Here σ is the associated range parameter, \mathbf{p} denotes the momentum of the relative motion of an atom pair, and $p = |\mathbf{p}|$ is its modulus. The model parameters ζ and σ are determined mainly by the resonance width ΔB of Eq. (2) and the resonance shift $B_0 - B_{\text{res}}$ [19]. Interchannel coupling is also responsible for the avoided crossing of the levels E_{-1}^{d} and E_{-2}^{d} , illustrated in Figs. 2 and 10.

b. Background scattering

The background-scattering potential V_{bg} describes the interaction of a pair of entrance-channel atoms in the absence of interchannel coupling at magnetic fields asymptotically far away from diatomic zero-energy resonances. In combination with the resonance state, its bare vibrational energy levels determine the number and main properties of comparatively tightly bound dressed, two-channel target states for three-body recombination at negative a . Their significance tends to decrease with increasing binding energy. Whereas realistic alkali atom pair potentials typically support dozens of dimer levels, we found it sufficient to account for only the two highest excited vibrational states in our model of V_{bg} to determine the correct magnitudes of $K_3(B)$ in Fig. 3. To this end it is crucial, however, to precisely mimic the properties of the dressed dimer energy levels E_{-1}^{d} and E_{-2}^{d} indicated in Figs. 2 and 10, which have been inferred from exact coupled-channels calculations [27].

Similarly to the interchannel coupling, the precise functional form of the microscopic potential $V_{\text{bg}}(r)$ is unresolved for the energy range of interest, leaving a choice of models predicting the same physics. To describe background scattering as well as the two highest excited vibrational levels of $V_{\text{bg}}(r)$ we employ the following separable representation [67, 68] of the background-scattering potential:

$$V_{\text{bg}} = \sum_{j=1}^2 |\chi_j\rangle \xi_j \langle \chi_j|, \quad (\text{A31})$$

Such pseudo-interactions are particularly useful in numerically exact treatments of the three-body Schrödinger equation and can be strictly motivated by complete separable expansions of diatomic transition matrices [57, 69]. In accordance with Ref. [66], we choose each form factor $|\chi_j\rangle$ of Eq. (A31) to be a Gaussian function in momentum space:

$$\chi_j(p) = \langle \mathbf{p} | \chi_j \rangle = \frac{e^{-p^2 \sigma_j^2 / (2\hbar^2)}}{(2\pi\hbar)^{3/2}}. \quad (\text{A32})$$

The amplitudes ξ_j and range parameters σ_j are determined for $j = 1, 2$ in such a way that Eq. (A31) recovers a_{bg} of Eq. (2),

the effective range of the microscopic background-scattering potential [70, 71], as well as its two highest excited vibrational energy levels.

Given the resonance state energy $E_{\text{res}}(B)$ of Eq. (A28), Eqs. (A29), (A30), (A31) and (A32) completely set up our single-resonance model of the pair interaction (A27). We note that the associated diatomic two-channel bound-state energies do not depend on the functional form of $\phi_{\text{res}}(r)$ [19], whereas, in general, calculations of K_3 loss-rate constants could be sensitive to it. It turns out that the orthogonality assumption of Eq. (A26) allows us to treat three-body recombination without specifying the wave function $\phi_{\text{res}}(r)$. Similar phenomena have been discussed in the context of pairing in ultracold Fermi gases [72]. The predictive power of our model has so far been demonstrated not only in applications to two-body physics [19], but also to resonance-enhanced three-body decay of ^{87}Rb Bose-Einstein condensates [23] as well as atom-dimer collisions [73]. In contrast to the broad diatomic ^{133}Cs and ^{85}Rb resonances of the present paper, the narrow ^{87}Rb 1007 G resonance of Refs. [23] and [73] is closed-channel dominated [19].

c. AGS integral equations

Given the pair interactions of the three-body Hamiltonian (A1), the general AGS equations (A24) can be converted into integral equations by multiplying them by ${}_{\alpha}\langle \mathbf{q}, \mathbf{p} |$ from the left and inserting the completeness relation,

$$\int d\mathbf{p} \int d\mathbf{p}' \langle \mathbf{p} | \mathbf{q}, \mathbf{p}' \rangle_{\gamma} \langle \mathbf{q}, \mathbf{p}' | = 1, \quad (\text{A33})$$

for each $\gamma \neq \alpha$ into the sum on the right-hand side. Using a partial wave expansion, the numerical solution of Eq. (A24) is equivalent to matrix inversion on a two-dimensional grid involving both Jacobi momenta $q = |\mathbf{q}|$ and $p = |\mathbf{p}|$. This procedure is commonly known as the momentum space Faddeev approach [74].

Similarly to the usual separable-potential approach [57, 69], it is the particular form of Eq. (A27) in combination with Eq. (A26) that allow us to reduce this problem to a one-dimensional integral equation in the variable q . To this end, we introduce the following complete transition amplitudes,

$$\begin{aligned} \tilde{X}_{\text{bg},j}(\mathbf{q}) &= \frac{1}{3} \sum_{\alpha=1}^3 {}_{\alpha}\langle \mathbf{q}, \chi_j, \text{bg} | G_{\alpha}(z) | \psi_{\alpha,1} \rangle, \\ \tilde{X}_{\text{cl}}(\mathbf{q}) &= \frac{1}{3} \sum_{\alpha=1}^3 {}_{\alpha}\langle \mathbf{q}, \phi_{\text{res}}, \text{cl} | G_{\alpha}(z) | \psi_{\alpha,1} \rangle, \end{aligned} \quad (\text{A34})$$

and inhomogeneous terms,

$$\begin{aligned} \tilde{X}_{\text{bg},j}^{\text{i}}(\mathbf{q}) &= \frac{1}{3} \sum_{\alpha=1}^3 {}_{\alpha}\langle \mathbf{q}, \chi_j, \text{bg} | G_{\alpha}(z) | \psi_{\alpha,1}^{\text{i}} \rangle, \\ \tilde{X}_{\text{cl}}^{\text{i}}(\mathbf{q}) &= \frac{1}{3} \sum_{\alpha=1}^3 {}_{\alpha}\langle \mathbf{q}, \phi_{\text{res}}, \text{cl} | G_{\alpha}(z) | \psi_{\alpha,1}^{\text{i}} \rangle. \end{aligned} \quad (\text{A35})$$

Here the summation over the index $\alpha = 1, 2, 3$ refers to the equivalence of particle arrangements due to the identical nature of the three Bose atoms. Given these amplitudes, multiplying the AGS equations (A24) by ${}_\alpha\langle \mathbf{q}, \chi_j, \text{bg} | G_\alpha(z)$ and ${}_\alpha\langle \mathbf{q}, \phi_{\text{res}}, \text{cl} | G_\alpha(z)$ from the left and summing over the index α yields the following integral equations:

$$\begin{aligned} \tilde{X}_{\text{bg},j}(\mathbf{q}) &= \tilde{X}_{\text{bg},j}^i(\mathbf{q}) + \sum_{k=1}^2 \int d\mathbf{q}' \tilde{\mathcal{K}}_{jk}^{\text{bg,bg}}(\mathbf{q}, \mathbf{q}') \tilde{X}_{\text{bg},k}(\mathbf{q}') \\ &\quad + \int d\mathbf{q}' \tilde{\mathcal{K}}_j^{\text{bg,cl}}(\mathbf{q}, \mathbf{q}') \tilde{X}_{\text{cl}}(\mathbf{q}'), \\ \tilde{X}_{\text{cl}}(\mathbf{q}) &= \tilde{X}_{\text{cl}}^i(\mathbf{q}) + \sum_{k=1}^2 \int d\mathbf{q}' \tilde{\mathcal{K}}_k^{\text{cl,bg}}(\mathbf{q}, \mathbf{q}') \tilde{X}_{\text{bg},k}(\mathbf{q}') \\ &\quad + \int d\mathbf{q}' \tilde{\mathcal{K}}_{\text{cl,cl}}(\mathbf{q}, \mathbf{q}') \tilde{X}_{\text{cl}}(\mathbf{q}'). \end{aligned} \quad (\text{A36})$$

Here the index j assumes the values 1 and 2 and the integral kernels are given by the following expressions:

$$\begin{aligned} \tilde{\mathcal{K}}_{jk}^{\text{bg,bg}}(\mathbf{q}, \mathbf{q}') &= 2 {}_2\langle \mathbf{q}, \chi_j, \text{bg} | G_2(z) | \mathbf{q}', \chi_k, \text{bg} \rangle_1 \xi_k, \\ \tilde{\mathcal{K}}_j^{\text{bg,cl}}(\mathbf{q}, \mathbf{q}') &= 2 {}_2\langle \mathbf{q}, \chi_j, \text{bg} | G_2(z) | \mathbf{q}', \chi, \text{bg} \rangle_1 \zeta, \\ \tilde{\mathcal{K}}_k^{\text{cl,bg}}(\mathbf{q}, \mathbf{q}') &= 2 {}_2\langle \mathbf{q}, \phi_{\text{res}}, \text{cl} | G_2(z) | \mathbf{q}', \chi_k, \text{bg} \rangle_1 \xi_k, \\ \tilde{\mathcal{K}}_{\text{cl,cl}}(\mathbf{q}, \mathbf{q}') &= 2 {}_2\langle \mathbf{q}, \phi_{\text{res}}, \text{cl} | G_2(z) | \mathbf{q}', \chi, \text{bg} \rangle_1 \zeta. \end{aligned} \quad (\text{A37})$$

The indices $\alpha = 2$ and $\gamma = 1$ of the final and initial particle arrangements in these integral kernels are arbitrary as long as they differ, and the prefactors of 2 stem from the summation over indices $\gamma \neq \alpha$ in the general AGS equations (A24). As the kernels (A37) do not couple different partial waves associated with \mathbf{q} , Eqs. (A36) can be treated, in general, as independent sets of integral equations in the variable $q = |\mathbf{q}|$ for each partial wave individually. Since we have restricted ourselves to zero-energy initial conditions ($z = i0$) the inhomogeneous terms are isotropic, i.e. $\tilde{X}_{\text{bg},j}^i(\mathbf{q}) = \tilde{X}_{\text{bg},j}^i(q)$ and $\tilde{X}_{\text{cl}}^i(\mathbf{q}) = \tilde{X}_{\text{cl}}^i(q)$. Consequently, for all applications in this paper Eqs. (A36) involve the s -wave only.

d. Numerical treatment of the AGS integral equations

Due to the arrangement-channel Green's function, $G_2(z)$, the kernels of Eqs. (A37) have poles at the physical energies associated with dressed, coupled-channels bound states, as indicated in the upper panel of Fig. 2. In order to explicitly locate the positions of these singularities, we introduce the effective diatomic energy variable of the relative motion, $E = z - 3q^2/(4m)$, as well as the entrance-channel Green's function,

$$\hat{G}_{\text{bg}}(E) = (E + \hbar^2 \nabla^2 / m - V_{\text{bg}})^{-1}. \quad (\text{A38})$$

According to Ref. [66], the resonance denominator of the complete diatomic Green's function $G_2(z)$ is given by

$$\mathcal{E}(B, E) = E - E_{\text{res}}(B) - |\zeta|^2 \langle \chi | \hat{G}_{\text{bg}}(E) | \chi \rangle. \quad (\text{A39})$$

At each magnetic-field strength B , its zeros determine the locations of all diatomic bound-state energies $E_d = E_d(B)$ through $\mathcal{E}(B, E_d) = 0$. The dressed, coupled-channels dimer states are characterized by the wave-function normalization coefficient,

$$Z(B, E) = \frac{1}{\frac{\partial}{\partial E} \mathcal{E}(B, E)}, \quad (\text{A40})$$

which determines their closed-channel admixtures in the lower panel of Fig. 2 via the relation $Z(B) = Z(B, E_d)$. This coefficient in combination with the arrangement-channel Green's function and its resonance denominator determine the final state of Eq. (A25) to be

$$|\mathbf{q}, \phi_d\rangle_\alpha = G_\alpha(z) |\mathbf{q}, \phi_{\text{res}}, \text{cl}\rangle_\alpha \mathcal{E}(B, E) \sqrt{Z(B, E)} \quad (\text{A41})$$

in the limit $E \rightarrow E_d(B)$.

Besides the poles in Eqs. (A35) and (A37) at the diatomic bound-state energies, the resonance denominator of Eq. (A39) as well as the coefficient of Eq. (A40) involve singularities due to the bare Green's function of Eq. (A38). Although these unphysical singularities associated with bare vibrational levels cancel exactly in the AGS integral equations (A36), for any numerical implementation of Eqs. (A36) it is imperative to explicitly treat these cancellations. To this end, we introduce the modified, dimensionless transition amplitudes,

$$\begin{aligned} X_{\text{bg},j}(q) &= q \tilde{X}_{\text{bg},j}(q) \frac{\mathcal{E}(B, E)}{\sqrt{\langle \chi_j | \chi_j \rangle}} \sqrt{Z(B, E)}, \\ X_{\text{cl}}(q) &= q \tilde{X}_{\text{cl}}(q) \mathcal{E}(B, E) \sqrt{Z(B, E)}, \end{aligned} \quad (\text{A42})$$

in addition to the following inhomogeneous terms:

$$\begin{aligned} X_{\text{bg},j}^i(q) &= q \tilde{X}_{\text{bg},j}^i(q) \frac{\mathcal{E}(B, E)}{\sqrt{\langle \chi_j | \chi_j \rangle}} \sqrt{Z(B, E)}, \\ X_{\text{cl}}^i(q) &= q \tilde{X}_{\text{cl}}^i(q) \mathcal{E}(B, E) \sqrt{Z(B, E)}. \end{aligned} \quad (\text{A43})$$

Here the index j assumes the values 1 and 2, similarly to Eqs. (A34) and (A35). The associated AGS integral equations can be readily obtained from Eqs. (A36), which yields:

$$\begin{aligned} X_{\text{bg},j}(q) &= X_{\text{bg},j}^i(q) + \sum_{k=1}^2 \int_0^\infty dq' \mathcal{K}_{jk}^{\text{bg,bg}}(q, q') X_{\text{bg},k}(q') \\ &\quad + \int_0^\infty dq' \mathcal{K}_j^{\text{bg,cl}}(q, q') X_{\text{cl}}(q'), \\ X_{\text{cl}}(q) &= X_{\text{cl}}^i(q) + \sum_{k=1}^2 \int_0^\infty dq' \mathcal{K}_k^{\text{cl,bg}}(q, q') X_{\text{bg},k}(q') \\ &\quad + \int_0^\infty dq' \mathcal{K}_{\text{cl,cl}}(q, q') X_{\text{cl}}(q'). \end{aligned} \quad (\text{A44})$$

Here the modified kernels are given in terms of Eqs. (A37) by

the following expressions:

$$\begin{aligned}
\mathcal{K}_{jk}^{\text{bg,bg}}(q, q') &= qq' \sqrt{\frac{Z(B, E)}{Z(B, E')} \frac{\mathcal{E}(B, E)}{\mathcal{E}(B, E')}} \xi_k \sqrt{\frac{\langle \chi_k | \chi_k \rangle}{\langle \chi_j | \chi_j \rangle}} \\
&\quad \times \int d\Omega' \tilde{\mathcal{K}}_{jk}^{\text{bg,bg}}(\mathbf{q}, \mathbf{q}'), \\
\mathcal{K}_j^{\text{bg,cl}}(q, q') &= qq' \sqrt{\frac{Z(B, E)}{Z(B, E')} \frac{\mathcal{E}(B, E)}{\mathcal{E}(B, E')}} \frac{\zeta}{\sqrt{\langle \chi_j | \chi_j \rangle}} \\
&\quad \times \int d\Omega' \tilde{\mathcal{K}}_j^{\text{bg,cl}}(\mathbf{q}, \mathbf{q}'), \\
\mathcal{K}_k^{\text{cl,bg}}(q, q') &= qq' \sqrt{\frac{Z(B, E)}{Z(B, E')} \frac{\mathcal{E}(B, E)}{\mathcal{E}(B, E')}} \xi_k \sqrt{\langle \chi_k | \chi_k \rangle} \\
&\quad \times \int d\Omega' \tilde{\mathcal{K}}_k^{\text{cl,bg}}(\mathbf{q}, \mathbf{q}'), \\
\mathcal{K}_{\text{cl,cl}}(q, q') &= qq' \sqrt{\frac{Z(B, E)}{Z(B, E')} \frac{\mathcal{E}(B, E)}{\mathcal{E}(B, E')}} \zeta \\
&\quad \times \int d\Omega' \tilde{\mathcal{K}}_{\text{cl,cl}}(\mathbf{q}, \mathbf{q}'). \tag{A45}
\end{aligned}$$

Here $d\Omega'$ denotes the angular component of $d\mathbf{q}'$ and stems from the momentum integrals of Eqs. (A36).

The transformed one-dimensional AGS integral equations (A44) are numerically stable and can be readily solved for the complete transition amplitudes of Eqs. (A42). Using Eqs. (A16) and (A25), their solution determines the three-body recombination loss-rate constant via the following relation:

$$K_3 = 48\pi^2 (2\pi\hbar)^6 m \frac{q_f}{\hbar} \left| \frac{X_{\text{cl}}(q_f)}{q_f} \right|^2. \tag{A46}$$

Here the final Jacobi momentum q_f is given by Eq. (A17). Our implementation of the AGS method was used to determine the magnetic-field dependence of the K_3 loss-rate constants of Ref. [23] as well as in the upper panels of Figs. 3 and 6. A similar treatment using the same kernels but different inhomogeneous terms has been used to predict the scattering amplitudes for atom-dimer collisions in ultracold Bose gases of ^{87}Rb [23].

6. Parameters for ^{133}Cs Feshbach resonances

a. Diatomic entrance and closed channels

The nuclear spin quantum number $I = 7/2$ of ^{133}Cs [75] gives rise to two hyperfine manifolds labeled by the total atomic angular momentum quantum numbers, $F = 3$ and $F = 4$. Due to the magnetic field, each hyperfine level is split into Zeeman sublevels. Interatomic collisions in an ultracold gas are sensitive to the Zeeman state in which the atoms are prepared. Throughout this paper, this Zeeman state is characterized by the ($F = 3, m_F = +3$) angular momentum quantum numbers of the atomic state which it adiabatically correlates with in the limit of zero field. Due to the

spatially homogeneous nature of the magnetic field, all pair potentials are invariant with respect to rotations about the field axis. Both the high- and low-field ^{133}Cs Feshbach resonances studied in this paper interact with the diatomic entrance-spin-channel mainly via spin exchange [17, 65]. These interactions do not couple different partial waves associated with the relative motion of an atom pair. Consequently, the entrance-spin-channel, $(F_1, m_1; F_2, m_2) = (3, 3; 3, 3)$, associated with a pair of ^{133}Cs atoms 1 and 2 is coupled only to those Zeeman states which conserve the sum of single-particle angular momentum projection quantum numbers, $m_1 + m_2 = 6$. All possible strongly coupled closed channels are therefore characterized by the pairs of atomic quantum numbers $(3, 2; 4, 4)$, $(3, 3; 4, 3)$, $(4, 3; 4, 3)$, and $(4, 4; 4, 2)$. Their associated magnetic moments can be estimated by the Breit-Rabi formula [76] to determine the bare resonance-state energies $E_{\text{res}}(B)$ of Eq. (A28) [19].

b. Low-field zero-energy resonance

The low-field zero-energy resonance at the negative magnetic-field strength [26] of $B_0 = -11.2\text{G}$ is caused by a Feshbach resonance level, $E_{\text{res}}(B)$, comprised of Zeeman states mainly from the excited $F = 4$ hyperfine level. Independently of the specific spin composition of the associated strongly coupled closed-spin-channel state the Breit-Rabi formula yields $\mu_{\text{res}} = h \times 4.2\text{MHz/G}$ for the magnetic moment difference of Eq. (A28). Coupled-channels scattering calculations of the resonance-enhanced scattering length $a(B)$ including basis states of both s -wave and d -wave symmetries determine the parameters a_{bg} and ΔB given in Subsection II A. Besides a_{bg} , the energies of the two highest excited bare vibrational entrance-channel states of $-h \times 0.01\text{MHz}$ and $-h \times 111\text{MHz}$, as well as the effective range $r_{\text{eff}} = 252 a_0$ determine the separable background-scattering potential of Eq. (A31). Given the background-scattering length, both of the bare energies [70] as well as r_{eff} [70, 71] are determined mainly by the van der Waals dispersion coefficient $C_6 = 6890\text{a.u.}$ of cesium [39] (the atomic unit of C_6 is $1\text{a.u.} = 9.5734 \times 10^{-26}\text{Jnm}^6$). The resonance width ΔB and the shift $B_0 - B_{\text{res}} = -29\text{G}$ [19] determine our model of the interchannel coupling. All these physical parameters give the model parameters of Eqs. (A29), (A30), (A31), and (A32) to be: $\xi_1 = -5.4187 \times 4\pi^{3/2} \hbar^2 \sigma_1 / m$, $\xi_2 = -12.9603 \times 4\pi^{3/2} \hbar^2 \sigma_2 / m$, $\zeta = 0.59623807 \times 2\pi^{3/4} \hbar^2 / (m\sigma^{1/2})$, $\sigma_1 = 82.3601 a_0$, $\sigma_2 = 36.4963 a_0$, and $\sigma = 14.4694 a_0$.

c. High-field zero-energy resonance

The high-field zero-energy resonance at $B_0 = 800\text{G}$ exists due to strong coupling between the diatomic $(3, 3; 3, 3)$ entrance-spin-channel and a closed spin channel comprised of the $(3, 2; 4, 4)$ and $(3, 3; 4, 3)$ Zeeman-state configurations. According to coupled-channels calculations of the s -wave bound states, their relative admixtures to the closed-channel superposition state are about 57% and 43%, respectively.

Based on the Breit-Rabi formula, these admixtures imply an estimated magnetic-moment difference associated with the Feshbach-resonance state of $\mu_{\text{res}} = h \times 2.6 \text{ MHz/G}$. We note that due to the single-particle spin overlap between the entrance and closed channels, Eq. (A26) does not strictly apply to the 800 G high-field zero-energy resonance. We believe, however, that the associated sensitivity to short-distance physics, such as the functional form of the resonance state, $\phi_{\text{res}}(r)$, is sufficiently small for our calculations to predict the correct orders of magnitude of K_3 . Our estimates of three-body zero-energy resonance positions are unaffected by spin-overlap, as they only involve energy scales much closer to the dissociation threshold than three-body recombination into tightly bound diatomic target states at negative $a(B)$.

The physical parameters a_{bg} and ΔB determining the resonance-enhanced scattering length of Eq. (2) near 800 G are given in Subsection III A. Based on a_{bg} and C_6 we calculate the energies of the two highest excited vibrational levels of the bare background-scattering potential to be $-h \times 0.0086 \text{ MHz}$ and $-h \times 110 \text{ MHz}$, while the effective range and resonance shift amount to $r_{\text{eff}} = 255 a_0$ and $B_0 - B_{\text{res}} = -87 \text{ G}$, respectively. Accordingly, the model parameters of Eqs. (A29), (A30), (A31), and (A32) for the high-field zero-energy resonance are given by: $\xi_1 = -6.5718 \times 4\pi^{3/2} \hbar^2 \sigma_1 / m$, $\xi_2 = -13.7782 \times 4\pi^{3/2} \hbar^2 \sigma_2 / m$, $\zeta = 0.92953214 \times 2\pi^{3/4} \hbar^2 / (m\sigma^{1/2})$, $\sigma_1 = 80.6241 a_0$, $\sigma_2 = 38.512 a_0$, and $\sigma = 18.7179 a_0$.

-
- [1] V. Efimov, Phys. Lett. **33B**, 563 (1970).
 [2] V. Efimov, Sov. J. Nucl. Phys. **12**, 589 (1971).
 [3] A.S. Jensen, K. Riisager, D.V. Fedorov, and E. Garrido, Rev. Mod. Phys. **76**, 215 (2004).
 [4] L.H. Thomas, Phys. Rev. **47**, 903 (1935).
 [5] T.K. Lim, Sister K. Duffy, and W.C. Damer, Phys. Rev. Lett. **38**, 341 (1977).
 [6] E. Nielsen and J.H. Macek, Phys. Rev. Lett. **83**, 1566 (1999).
 [7] B.D. Esry, C.H. Greene, and J.P. Burke, Phys. Rev. Lett. **83**, 1751 (1999). The recombination cross section formula, Eq. (1), and also all of the calculated recombination rates in that Letter, should be reduced by a factor of 6. We thank José D’Incao, Brett Esry and Chris Greene for pointing this out to us.
 [8] T. Kraemer, M. Mark, P. Waldburger, J.G. Danzl, C. Chin, B. Engeser, A.D. Lange, K. Pilch, A. Jaakkola, H.-C. Nägerl, and R. Grimm, Nature (London) **440**, 315 (2006).
 [9] R.E. Grisenti, W. Schöllkopf, J.P. Toennies, G.C. Hegerfeldt, T. Köhler, and M. Stoll, Phys. Rev. Lett. **85**, 2284 (2000).
 [10] Th. Cornelius and W. Glöckle, J. Chem. Phys. **85**, 3906 (1986).
 [11] B.D. Esry, C.D. Lin, and C.H. Greene, Phys. Rev. A **54**, 394 (1996).
 [12] L.W. Bruch and K. Sawada, Phys. Rev. Lett. **30**, 25 (1973).
 [13] V. Efimov, Nucl. Phys. A **362**, 45 (1981).
 [14] W. Schöllkopf and J.P. Toennies, Science **266**, 1345 (1994).
 [15] R. Brühl, A. Kalinin, O. Kornilov, J.P. Toennies, G.C. Hegerfeldt, and M. Stoll, Phys. Rev. Lett. **95**, 063002 (2005).
 [16] W.C. Stwalley, Phys. Rev. Lett. **37**, 1628 (1976).
 [17] E. Tiesinga, B.J. Verhaar, and H.T.C. Stoof, Phys. Rev. A **47**, 4114 (1993).
 [18] S. Inouye, M.R. Andrews, J. Stenger, H.-J. Miesner, D.M. Stamper-Kurn, and W. Ketterle, Nature (London) **392**, 151 (1998).
 [19] T. Köhler, K. Góral, and P.S. Julienne, Rev. Mod. Phys. **78**, 1311 (2006).
 [20] M. Stoll and T. Köhler, Phys. Rev. A **72**, 022714 (2005).
 [21] E. Braaten and H.-W. Hammer, Phys. Rev. Lett. **87**, 160407 (2001).
 [22] E. Braaten and H.-W. Hammer, Phys. Rep. **428**, 259 (2006).
 [23] G. Smirne, R.M. Godun, D. Cassettari, V. Boyér, C.J. Foot, T. Volz, N. Syassen, S. Duerr, G. Rempe, M.D. Lee, K. Góral, and T. Köhler, Phys. Rev. A **75**, 020702 (2007).
 [24] J.R. Taylor, *Scattering Theory* (Wiley, New York, 1972).
 [25] A.J. Moerdijk, B.J. Verhaar, and A. Axelsson, Phys. Rev. A **51**, 4852 (1995).
 [26] J.M. Vogels, B.J. Verhaar, and R.H. Blok, Phys. Rev. A **57**, 4049 (1998).
 [27] C. Chin, V. Vuletić, A.J. Kerman, S. Chu, E. Tiesinga, P.J. Leo, and C.J. Williams, Phys. Rev. A **70**, 032701 (2004).
 [28] T. Weber, J. Herbig, M. Mark, H.-C. Nägerl, and R. Grimm, Phys. Rev. Lett. **91**, 123201 (2003).
 [29] H.-C. Naegerl, T. Kraemer, M. Mark, P. Waldburger, J.G. Danzl, B. Engeser, A.D. Lange, K. Pilch, A. Jaakkola, C. Chin, and R. Grimm, e-print cond-mat/0611629.
 [30] M.V. Zhukov, B.V. Danilin, D.V. Fedorov, J.M. Bang, I.J. Thompson, and J.S. Vaagen, Phys. Rep. **231**, 151 (1993).
 [31] A. Kalinin, O. Kornilov, W. Schöllkopf, and J.P. Toennies, Phys. Rev. Lett. **95**, 113402 (2005).
 [32] E. Braaten and H.-W. Hammer, Phys. Rev. A **67**, 042706 (2003).
 [33] M.L.E. Oliphant, P. Harteck, and E. Rutherford, Proc. Roy. Soc. (London) A **144**, 692 (1934).
 [34] S.K. Adhikari and L. Tomio, Phys. Rev. C **26**, 83 (1982).
 [35] V. Efimov, Phys. Rev. C **44**, 2303 (1991).
 [36] V. Efimov, Phys. Rev. C **47**, 1876 (1993).
 [37] E. Braaten and H.-W. Hammer, Phys. Rev. Lett. **91**, 102002 (2003).
 [38] E. Braaten and H.-W. Hammer, e-print cond-mat/0610116v1.
 [39] P.J. Leo, C.J. Williams, and P.S. Julienne, Phys. Rev. Lett. **85**, 2721 (2000).
 [40] J.L. Roberts, N.R. Claussen, S.L. Cornish, and C.E. Wieman, Phys. Rev. Lett. **85**, 728 (2000).
 [41] S.L. Cornish, N.R. Claussen, J.L. Roberts, E.A. Cornell, and C.E. Wieman, Phys. Rev. Lett. **85**, 1795 (2000).
 [42] T. Weber, J. Herbig, M. Mark, H.-C. Nägerl, and R. Grimm, Science **299**, 232 (2003).
 [43] J.P. D’Incao, H. Suno, and B.D. Esry, Phys. Rev. Lett. **93**, 123201 (2004).
 [44] J.P. D’Incao and B.D. Esry, Phys. Rev. A **73**, 030703(R) (2006).
 [45] R.D. Amado and J.V. Noble, Phys. Rev. D **5**, 1992 (1972).
 [46] R.G. Newton, *Scattering Theory of Waves and Particles* (Springer, New York, 1982).
 [47] N.R. Claussen, S.J.J.M.F. Kokkelmans, S.T. Thompson, E.A. Donley, E. Hodby, and C.E. Wieman, Phys. Rev. A **67**, 060701(R) (2003).
 [48] S.T. Thompson, E. Hodby, and C.E. Wieman, Phys. Rev. Lett. **95**, 190404 (2005).
 [49] S. Jonsell, H. Heiselberg, and C.J. Pethick, Phys. Rev. Lett. **89**,

- 250401 (2002).
- [50] F. Werner and Y. Castin, Phys. Rev. Lett. **97**, 150401 (2006); Phys. Rev. A **74**, 053604 (2006).
- [51] T. Luu and A. Schwenk, Phys. Rev. Lett. **98**, 103202 (2007).
- [52] T. Köhler, E. Tiesinga, and P.S. Julienne, Phys. Rev. Lett. **94**, 020402 (2005).
- [53] E. Nielsen, H. Suno, and B.D. Esry, Phys. Rev. A **66**, 012705 (2002).
- [54] S. Jonsell, Europhys. Lett. **76**, 8 (2006).
- [55] H.T.C. Stoof, B.J. Verhaar, L.P.H. de Goey, and W. Glöckle, Phys. Rev. B **40**, 9176 (1989).
- [56] E.O. Alt, P. Grassberger, and W. Sandhas, Nucl. Phys. B **2**, 167 (1967).
- [57] W. Sandhas, Acta Phys. Austriaca, Suppl. **IX**, 57 (1972).
- [58] A.J. Moerdijk, H.M.J.M. Boesten, and B.J. Verhaar, Phys. Rev. A **53**, 916 (1996).
- [59] Y. Kagan, B.V. Svistunov, and G.V. Shlyapnikov, JETP Lett. **42**, 209 (1985).
- [60] E.A. Burt, R.W. Ghrist, C.J. Myatt, M.J. Holland, E.A. Cornell, and C.E. Wieman, Phys. Rev. Lett. **79**, 337 (1997).
- [61] H. Suno, B.D. Esry, C.H. Greene, and J.P. Burke, Phys. Rev. A **65**, 042725 (2002).
- [62] P. Soldán, M.T. Cvitaš, J.M. Hutson, P. Honvault, and J.-M. Launay, Phys. Rev. Lett. **89**, 153201 (2002).
- [63] J. Blandon, V. Kokouline, and F. Masnou-Seeuws, Phys. Rev. A **75**, 042508 (2007).
- [64] L.D. Faddeev, Soviet Phys. - JETP **12**, 1014 (1961).
- [65] H.T.C. Stoof, J.M.V.A. Koelman, and B.J. Verhaar, Phys. Rev. B **38**, 4688 (1988).
- [66] K. Góral, T. Köhler, S.A. Gardiner, E. Tiesinga, and P.S. Julienne, J. Phys. B **37**, 3457 (2004).
- [67] Y. Yamaguchi, Phys. Rev. **95**, 1628 (1954).
- [68] A.N. Mitra, Phys. Rev. **127**, 1342 (1962).
- [69] C. Lovelace, Phys. Rev. **135**, B1225 (1964).
- [70] B. Gao, Phys. Rev. A **58**, 4222 (1998).
- [71] V.V. Flambaum, G.F. Gribakin, and C. Harabati, Phys. Rev. A **59**, 1998 (1999).
- [72] C. Honerkamp and W. Hofstetter, Phys. Rev. B **70**, 094521 (2004); M.M. Parish, B. Mihaila, B.D. Simons, and P.B. Littlewood, Phys. Rev. Lett. **94**, 240402 (2005); G.M. Bruun, A.D. Jackson, and E.E. Kolomeitsev, Phys. Rev. A **71**, 052713 (2005).
- [73] N. Syassen, T. Volz, S. Teichmann, S. Dürr, and G. Rempe, Phys. Rev. A **74**, 062706 (2006).
- [74] W. Glöckle, *The Quantum Mechanical Few-Body Problem* (Springer, Berlin, 1983).
- [75] E. Arimondo, M. Inguscio, and P. Violino, Rev. Mod. Phys. **49**, 31 (1979).
- [76] G. Breit and I.I. Rabi, Phys. Rev. **38**, 2082 (1931).